Hindawi
Complexity
Volume 2021, Article ID 6697311, 23 pages
https://doi.org/10.1155/2021/6697311

Research Article

Analysis of Control Characteristics and Design of Control System Based on Internal Parameters in Doubly Fed Variable-Speed Pumped Storage Unit

Guopeng Zhao,[1,2] **Yongxin Zhang**,[2] **and Jiyun Ren**[2]

[1]*State Key Laboratory of Alternate Electrical Power System with Renewable Energy Sources, North China Electric Power University, Beijing 102206, China*
[2]*School of Electrical and Electronic Engineering, North China Electric Power University, Beijing 102206, China*

Correspondence should be addressed to Guopeng Zhao; zhaoguopeng@ncepu.edu.cn

Received 16 November 2020; Revised 14 April 2021; Accepted 1 June 2021; Published 17 June 2021

Academic Editor: Alex Alexandridis

Copyright © 2021 Guopeng Zhao et al. This is an open access article distributed under the Creative Commons Attribution License, which permits unrestricted use, distribution, and reproduction in any medium, provided the original work is properly cited.

In this paper, the control strategies and their characteristics when applied to the doubly-fed variable-speed pumped storage unit in generating mode and pump mode are discussed. The composition of doubly fed variable-speed pumped storage unit is introduced, and the mathematical model of every component is proposed. Two control strategies of the unit are introduced. One is the power priority control strategy and the other is the speed priority control strategy. Then, the control block diagrams of the two control strategies in the generating mode and the pump mode are established, and the parameters of the unit in each control strategy are designed. The two control strategies are simulated in power generation and pumping conditions. Finally, the conclusion that power priority strategy has a better effect on power control is obtained.

1. Introduction

With the large-scale development of renewable energy generation, such as wind power and photovoltaic energy [1, 2], the balance of the power system is facing great challenges. The power handling capability of the energy storage system is utilized to achieve balance in the power system, thereby ensuring the safe and stable operation of the power system, which has become an important breakthrough for the current sustainable development of the power grid [3]. Pumped-storage power stations have functions such as peak regulation, vacancies compensation, frequency regulation, phase regulation, and accident standby. It can be used to smooth the output of renewable energy on a large scale [4], which has great significance to solve the problem of safe and stable operation of the power grid caused by the large-scale development of new energy sources such as wind power [5].

The realization of variable speed pumped storage is one of the most important advances in this field in recent decades. Compared with the traditional fixed-speed unit, variable-speed pumped-storage unit can adjust the unit's speed according to the change of head and flow in the generating mode and the pump mode, so that the unit is always at optimal efficiency speed which can improve unit operating efficiency [6]. Besides, high-speed decoupling control of active power and reactive power can be realized. Variable-speed pumped-storage unit can better adapt to different operating heads, which also can improve the hydraulic performance of pump turbine; reduce vibration, cavitation, and sand wear; expand the operating range; and improve unit stability [7–10]. At present, there are two main realization forms of variable-speed pumped-storage units, which includes DFVSPS (doubly fed variable-speed pumped storage) and direct-drive variable-speed pumped storage [11, 12]. And, the technology of DFVSPS is widely used.

The research content of the DFVSPS unit is extensive at present. For example, the compensation effect of DFVSPS units on output fluctuations of renewable energy generation such as wind power and photovoltaic energy is studied in

literature [13, 14]. Some literatures have studied the converters and power electronics of the DFVSPS unit [15–17]. In addition, some literatures have studied the characteristics of the doubly fed variable-speed pumped-storage unit in the event of a failure [18, 19]. The DFVSPS unit is a huge system, including pump turbine, doubly fed induction motor (DFIM), inverter, control system, etc. It will also cause many problems when it is applied to the power system, so there is still much to be thought about in the research of DFSPS unit.

For the research on the control characteristics of the DFVSPS unit, a large amount of literature focused on the realization of power decoupling control of the DFVSPS unit, mainly by establishing the mathematical model of each part of the unit, such as pump turbine, DFIM, and control system, then establishing a simulation program of the unit in the simulation software. After the unit enters the steady state, the control part of the rotor side converter is superimposed with the increase and decrease instruction of active power and reactive power, and whether the stator side power of the DFIM can track the change of instructions is observed [20, 21]. These studies mainly investigate whether the DFVSPS unit can respond to the superimposed power increase and decrease commands when it is operating in a steady state. The different response parameters and control methods in the power response process have not been analyzed in detail, and the effect of unit internal parameters on control characteristics has not been considered.

The overall methods to control the DFVSPS unit include power priority control strategy and speed priority control strategy. For the applicable working conditions to each control strategy, there is less relevant literature and no in-depth research has been conducted. There have been some research findings on pumped storage control. Their control strategy is not comprehensive and considers too few working conditions. The research content has little practical significance. Therefore, it is necessary to study the pumped storage energy control system more deeply [22]. Power priority control strategy was adopted in the generating mode and the pump mode of the No. 4 unit of the Ohkawachi Power Station in Japan [23]. In the literature [24], the control characteristics of the two control strategies in the generating mode were simulated and studied. The characteristics of each control strategy were described. The research is not carried out from the level of the unit control system. Thus, it is necessary to conduct in-depth research in the control characteristics of each control strategy.

This paper focuses on the control strategies and characteristics of the DFVSPS unit. Based on the unit internal parameters and control system, the characteristics of the DFVSPS unit are studied in depth. And, the follow-up research on the application of the DFVSPS unit in the power system is prepared. The second section of this paper introduces the composition, mathematical model, and control strategy of a DFVSPS unit. The third section mainly studies the influence of the internal parameters on the control characteristics of the unit. The fourth section analyzes and designs the control parameters of the unit according to the control system. The control characteristics of the two strategies in the generating and pump mode are compared, and the applicable conditions for each control strategy are obtained in the fifth section. The full text is summarized and relevant conclusions are drawn in the last section of this paper.

2. Unit Composition, Mathematical Model of Each Part, and Control Strategy

The unit compositions and methods section should contain sufficient detail so that all procedures can be repeated. It may be divided into headed subsections if several methods are described. The structure of the DFVSPS unit is shown in Figure 1, which is composed of the DFIM, pump turbine, and the converter and control system. The stator of the DFIM is connected to the grid, and the rotor side of the DFIM is connected to the grid through a converter. The control system includes a pump-turbine regulation system and a rotor side converter excitation control system.

In Figure 1, P_m is the mechanical power; P_s, Q_s are the active and reactive power of the DFIG stator side, respectively; P_r, Q_r are the active and reactive power of the DFIG rotor side, respectively; P_c, Q_c are the active and reactive power from the grid to the converter, respectively; and P_g, Q_g are the active and reactive power from the DFVSPS unit to the grid, respectively.

2.1. Mathematical Model of DFIM. In actual operation, the electromechanical energy conversion of the DFIM is mainly accomplished by a fundamental magnetic field. The general motor control also takes the magnetic flux, voltage, and current of the fundamental wave as the basis of motor control. In ideal conditions, the DFIM mathematical model in the three-phase rotating coordinate system is a high-order, nonlinear, time-varying, and strongly coupled system. So it is difficult to analyze and control the motor in ideal conditions. So, we convert the mathematical model from the three-phase rotating coordinate system to the two-phase rotating coordinate system through the coordinate transformations, and then the vector control strategy is used to analyze and control. In this paper, the stator voltage-oriented vector control strategy is adopted. The Voltage equation and Flux equation of the mathematical model of the DFIM in the two-phase rotating coordinate system is shown in literature [25].

Electromagnetic torque equation:

$$T_e = \frac{3}{2} p_n L_m \left(i_{\mathrm{sq}} i_{\mathrm{rd}} - i_{\mathrm{sd}} i_{\mathrm{rq}} \right), \tag{1}$$

where p_n is the number of poles.

Motion equation:

$$\frac{J}{p_n} \frac{\mathrm{d}\omega_m}{\mathrm{d}t} = T_e - T_m - B_m \omega_m, \tag{2}$$

where ω_m is the speed of the DFIM; J is rotational inertia of the DFIM; and B_m is the friction coefficient of the DFIM.

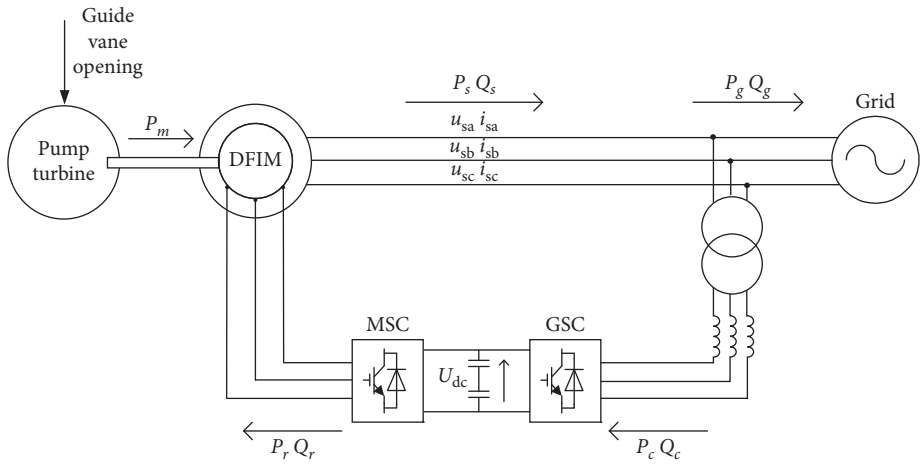

Figure 1: Structure diagram of the DFVSPS unit.

2.2. Mathematical Model of the Pump Turbine. Pump turbine is one of the important devices of the DFVSPS power station, which rotates in the positive direction in the turbine mode and in the reverse direction in the pump mode. Accurate model of the pump turbine is the basis for the study of unit control characteristics. However, due to the complex structure of the pump turbine, frequent changes of operating conditions during operation, the complex internal flow fields, water hammer, influence of cavitation erosion, and so on, , there is still no model that can fully characterize the operation characteristics of pump turbine. This is despite studies on this phenomenon by many scholars at home and abroad. The mathematical model of the pump turbine is generally expressed by the relationship among the mechanical torque T_m, the flow rate Q, the guide vane opening y, the water head H, and the speed n. At present, the universal model of the pump turbine is the full characteristic curve obtained through the model test. The full characteristic curve of the pump turbine is shown in literature [26].

The full characteristic curve can describe the characteristics of the pump turbine in various operating conditions, but it needs to be obtained by the model test. So, it is difficult to obtain the data, and the amount of calculation during interpolation calculation is large, which causes great difficulties in the research and analysis of the entire variable speed pumped storage unit. Therefore, this paper divides the pump turbine model into two parts as the model in the turbine mode and the model in the pump mode.

2.2.1. Pump Turbine Model in the Turbine Mode. In the turbine mode, the unit operates within the rated speed range, excluding the *S* zone caused by the runaway speed. The conventional turbine model can be used to replace the pump turbine model in the turbine mode [27]. In this paper, the simplified analytical nonlinear model proposed by the IEEE Working Group in 1992 [28] is adopted. According to the full characteristic curve of the pump turbine, the speed has little influence on the flow characteristics of pump turbine in low-speed zone, so ignore the impact. The model can be expressed by the following formula:

$$\begin{cases} q = y\sqrt{h}, \\ p_m = A_t(q - q_{\mathrm{nl}})h, \end{cases} \tag{3}$$

where P_m is the mechanical power, q_{nl} is the no-load flow rate, and A_t is the ratio of ideal guide vane opening to the actual guide vane opening.

The rigid water theory is used in the water diversion system, which can be derived as shown in the following formula:

$$\Delta h = -T_w \frac{\mathrm{d}q}{\mathrm{d}t}, \tag{4}$$

where T_w is the time constant of water flow inertia.

Considering that this paper mainly analyzes the control characteristics of the pump turbine running near the rated operating condition, the simplified nonlinear model is linearized at the rated operating point and the Laplace domain transformation is carried out to obtain the ideal pump turbine model in the rated operating condition as the following formula:

$$\frac{\Delta p_m}{\Delta y} = \frac{1 - T_w s}{1 + 0.5 T_w s}. \tag{5}$$

2.2.2. Pump Turbine in the Pump Mode. In the pump mode, when the unit is operating near the rated operating condition, the guide vane opening is large, and the full characteristic curves of the pump turbine seriously overlap. So, the guide vane opening has little effect on the flow of the pump turbine. At this time, there is a cubic relationship between the mechanical power of the pump turbine and its speed [29]. According to the pump affinity characteristics, the pump turbine model in the pump mode can be expressed as follows:

$$\frac{Q_1}{Q_2} = \frac{\omega_1}{\omega_2},$$
$$\frac{H_1}{H_2} = \left(\frac{\omega_1}{\omega_2}\right)^2, \quad (6)$$
$$\frac{P_{m_1}}{P_{m_2}} = \left(\frac{\omega_1}{\omega_2}\right)^3,$$

where subscript 1, 2 indicate working points at two different speeds.

2.3. Excitation System and the Pump Turbine Adjustment System

2.3.1. Excitation System. The excitation system of the DFIM is composed of AC (alternating current)-DC (direct current)-AC converter. The grid-side converter is connected to the power grid through an excitation transformer and its main control objective is to maintain the DC bus voltage. The machine-side converter is connected to the rotor side of the DFIM, which mainly accomplishes the control to the active power, reactive power, and electromagnetic torque of the DFIM. The topology structure and control method of the machine-side converter and grid-side converter are shown in Figure 2.

2.3.2. Pump Turbine Adjustment System. The structure of the adjustment system of the pump turbine is shown in Figure 3. In this paper, a classic PI controller is adopted as the governor. The function of the electrohydraulic servo system is to convert the electrical signal of the governor into a mechanical signal for output, thereby controlling the guide vane opening. The common servo system is AC servo motor/electrohydraulic actuator servo system, whose structure is shown in Figure 4. After the nonlinear links such as saturation limiting of a servomotor, dead zone, and gap nonlinearity are ignored, the servo system can be simplified to the following formula:where y_{pi} is the output of the guide vane opening of the governor; y is the output of the guide vane opening of the servo system; and y_1 is the output of the guide vane opening of the AC servo mechanism. There is a dead zone of governor output and a saturation limiting of main servomotor. T_{y_1} is the AC servo mechanism response time constant; T_y is the main servomotor time constant. In this paper, $T_{y_1} = 0.07$ and $T_y = 1$.

$$\frac{y(s)}{y_{\mathrm{pi}}(s)} = \frac{1}{T_y s\left(T_{y_1} s + 1\right) + 1}. \quad (7)$$

2.4. Control Strategy of the DFVSPS Unit. The traditional fixed-speed pumped storage unit can only operate at a synchronous speed. The unit cannot run at its optimal speed in the turbine mode, resulting in low efficiency and cavitation erosion, and its mechanical power cannot be adjusted in the pump mode. The DFVSPS unit can realize variable speed operation within a certain range by using DFIM and AC-DC-AC converter excitation system, which can improve the operation efficiency of the unit and realize the power regulation in the pump mode. There are two adjustable variables of the DFVSPS unit, namely, the unit speed and the unit power. The two adjustable variables can be adjusted, respectively, by the pump turbine adjustment system and the DFIM excitation system. Therefore, the unit has two control strategies, namely, power priority control strategy and speed priority control strategy.

2.4.1. Power Priority Control Strategy. The DFIM excitation adjustment system belongs to the electrical system, which adjusts quickly. The adjustment system of the pump-turbine guide vane opening realizes adjustment through a hydraulic system and a mechanical system, which adjusts slowly. Therefore, the strategy by which the power of the unit is adjusted in the DFIM excitation system, and the speed of the unit is regulated by the pump-turbine guide vane opening adjustment system, is the power priority control strategy. In this strategy, when the unit power reference value changes, the excitation system responds quickly, and the unit power quickly tracks the reference value. At the same time, the optimal speed calculation link calculates the optimal efficiency corresponding speed according to the full characteristic curve of the pump turbine, and transmits it to the guide vane opening adjustment system to achieve the control of the unit speed. The control strategy diagram of the power priority control strategy is shown in Figure 5 [30].

2.4.2. Speed Priority Control Strategy. Correspondingly, in the speed priority control strategy, the unit speed is controlled by the excitation system, and the unit power is controlled by the adjustment system of the guide vane opening. In this control strategy, when the power reference value of the unit changes, the speed corresponding to the optimal efficiency is calculated by the optimal speed calculation link firstly with the full characteristic curve of the pump turbine and the power reference value. The unit speed is adjusted by the excitation system. In the meantime, the unit power is regulated by the guide vane opening adjustment system according to the power reference value to make it stable near the reference value. The control strategy diagram of speed priority control strategy is shown in Figure 6 [30].

3. Analysis of the Influence of Unit Internal Parameters on Control Characteristics

According to the control strategy diagrams of the two control strategies, it can be found that the control characteristics of the unit are related to the parameters of the pump turbine (the water flow inertia time constant T_w, the selection of the speed range, the selection of the flying speed, etc.), the parameters of the DFIM (selection of inductance resistance parameters, selection of moment of inertia, etc.),

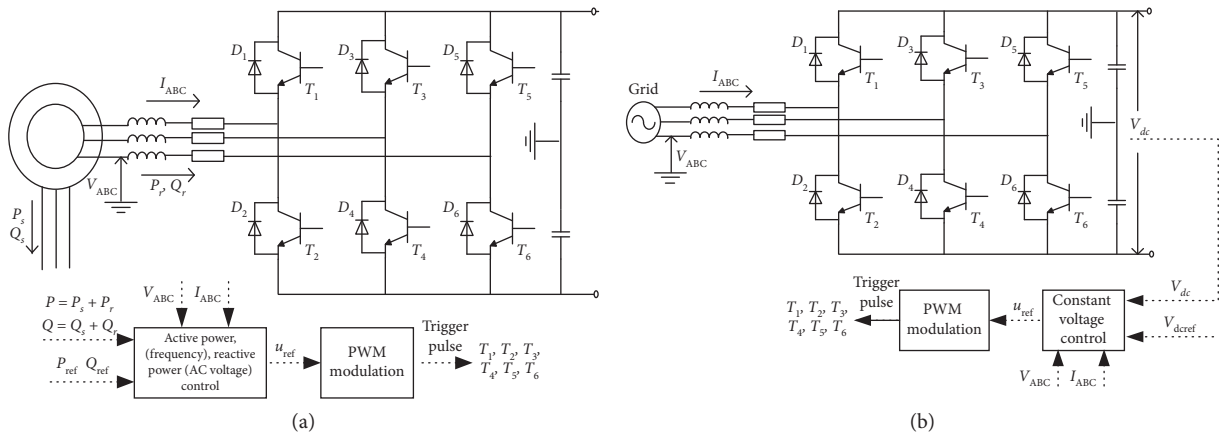

Figure 2: Topology structure and control method of the converter. (a) Topology structure and control method of the machine-side converter. (b) Topology structure and control method of the grid-side converter.

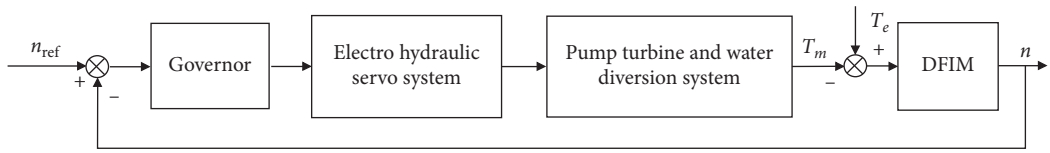

Figure 3: Adjustment system of the pump turbine.

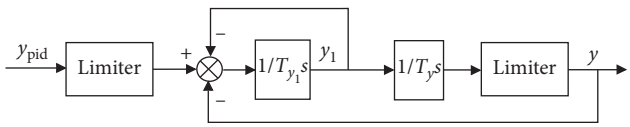

Figure 4: AC servo motor/electrohydraulic actuator type servo system.

the control parameters of the pump turbine adjustment system, and the control parameters of excitation control system.

The influence of the unit's own parameters (the parameters of the pump turbine and the parameters of the DFIM) on the control characteristics is firstly analyzed in this section, and the unit's parameters are designed. This section takes the analysis of the influence of the unit's parameters on the control characteristics as an example, when the power priority control strategy is used in the generating mode. The analysis of other conditions is similar to this, so this article will not repeat them. According to the control strategy diagram and the mathematical model of the unit, the block diagram of the power priority control strategy is shown in Figure 7, which is adopted in the generating mode.

3.1. Analysis of the Influence of Pump Turbine Parameters on Control Characteristics

3.1.1. Water Flow Inertia Time Constant T_w. T_w represents the time required for the water flow in the water diversion pipeline to increase from zero to the rated flow Q_r when the head is rated head H_r, which represents the water flow inertia in the water passing pipeline. The derivation of the T_w calculation is in the literature [31]. The formula is as follows:

$$T_w = \frac{Q_r}{gH_r} \sum \frac{L}{S} = \sum \frac{Lv}{gH_r}. \tag{8}$$

Among them: S is the cross-sectional area of each section of the pipeline, m^2; L is the corresponding length of each section of the overwater pipe, m; v is the corresponding flow rate in each section of the passage, m/s; Q_r is the rated flow rate of the turbine, m^3/s; H_r is the rated head, m; g is the gravitational acceleration, m/s^2; T_w's unit is second.

The T_w is related to the design of the water diversion system of the hydropower station. Generally, the larger the value of T_w, the greater the flow inertia, the greater the water hammer effect, the worse the stability, the greater the overshoot, the longer the adjustment time, so that the quality of the adjustment process deteriorates. The analysis is shown as follows. After analysis, this paper takes $T_w = 0.5$ s.

Figure 8 shows the zero-pole variation of the closed-loop transfer function of the rotational speed closed-loop when the water flow inertia time constant T_w changes. When T_w changes, there is always a zero point in the right half plane. Changing of T_w will change the position of the zero point in the right half plane, but a negative regulation will always be generated. The size of the negative regulation is affected by the change of the T_w. When other parameters are unchanged and the value of T_w is small, the conjugate pole is in the left half plane. As T_w increases, it transitions to the right half plane. Therefore, the larger T_w means the greater fluctuation of the speed closed-loop response and the more difficult to stabilize.

As shown in Figure 9, when other parameters of the control system remain unchanged and the water flow inertia time constant T_w changes, the power instruction increases

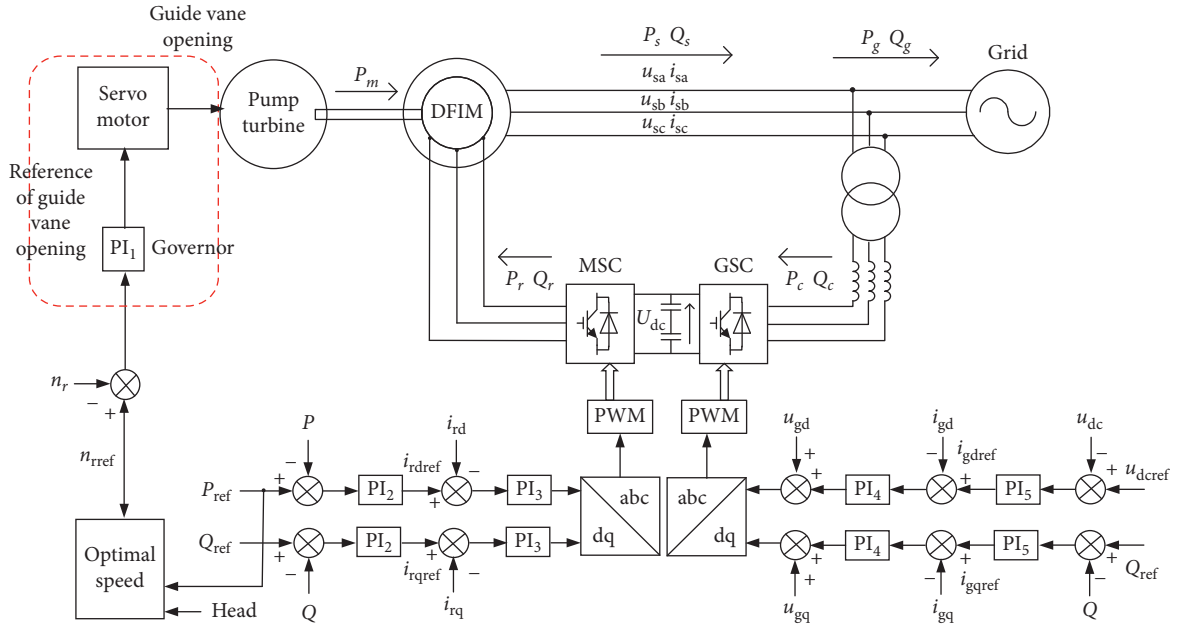

Figure 5: Control strategy diagram of the power priority control strategy.

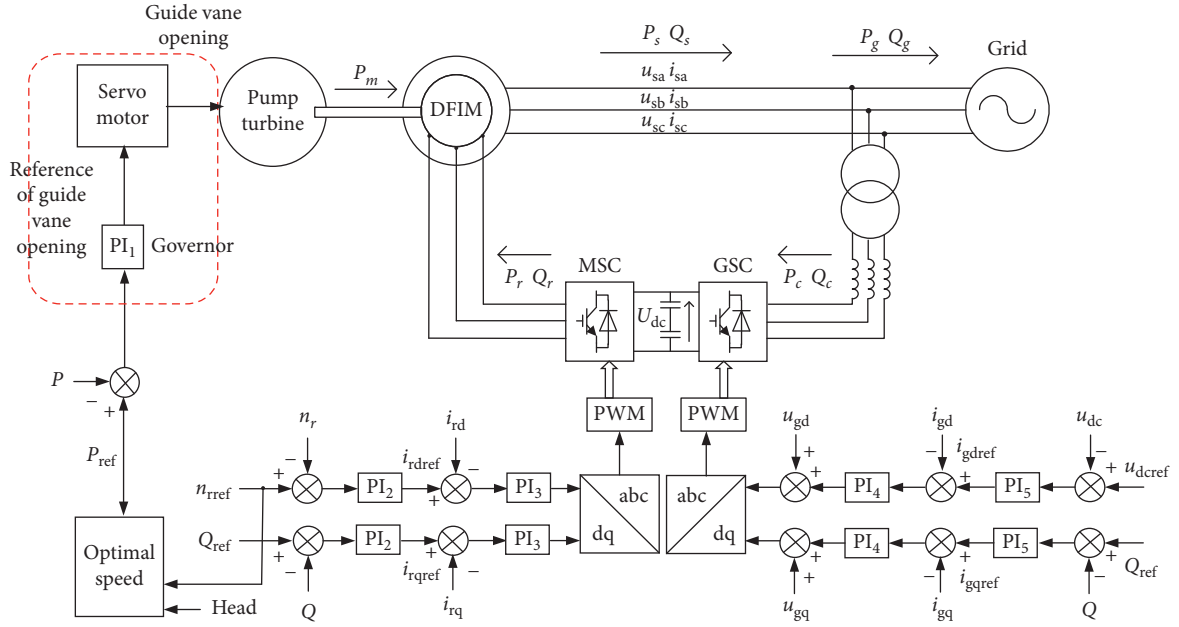

Figure 6: Control strategy diagram of the speed priority control strategy.

by 20 MW and the unit transmits the active power P_g to the power grid. It can be seen that the larger the T_w setting, the more obvious the power fluctuation and the longer adjustment time during the same adjustment process.

3.1.2. Range of Speed. For a pump turbine, the output of the pump turbine has a great relationship with the adjustable range of the speed of the pump turbine. After determining the adjustable range of the speed of the pump turbine, the output range will be determined according to the full characteristic curve of the pump turbine. The speed adjustment range of DFVSPS units is generally ±4% to ±10% according to the capacity of pumped storage power stations, which is mainly limited by the capacity of the converter.

3.1.3. Runaway Speed. It refers to the sudden drop of load due to unit failure during operation of the hydro-generator. The output power of the generator is zero. At this time, if the structure of the hydroturbine governor fails or the water guiding mechanism cannot be closed, the speed of the

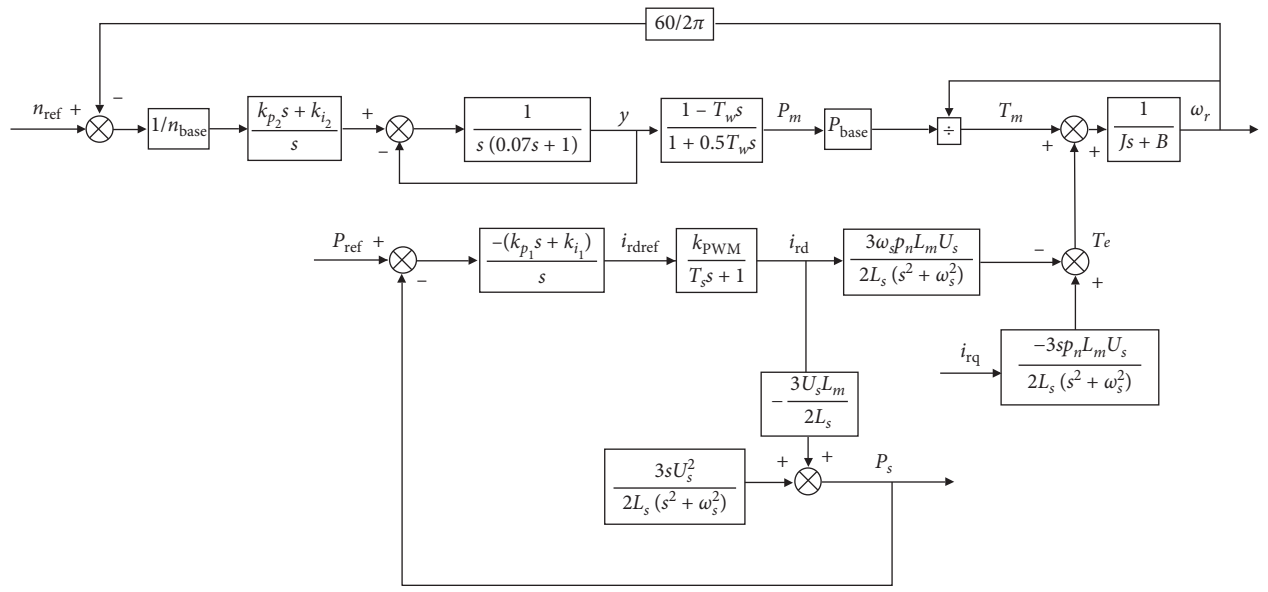

Figure 7: Control block diagram of the power priority control strategy in generating mode.

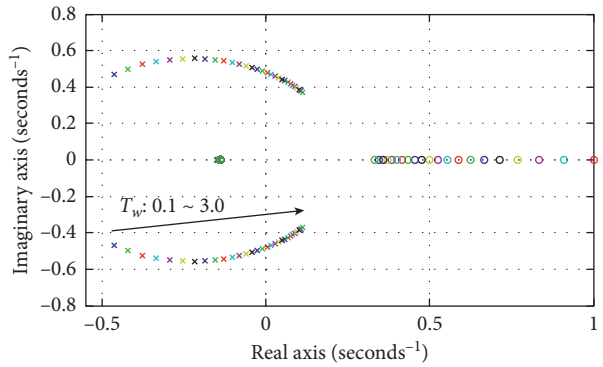

Figure 8: Zero-pole variation of the closed-loop transfer function of the rotational speed closed-loop when the water flow inertia time constant T_w changes.

hydro-turbine rises rapidly. The maximum speed that the unit can reach is called the runaway speed of the pump turbine.

When the load of the pumped storage unit is adjusted, the rotation speed of the shaft will fluctuate due to the difference between the output power of the pump turbine and the electromagnetic power of the DFIM. Therefore, it is necessary to study whether the speed will exceed the upper limit of the unit speed or is lower than the lower limit of the unit speed.

3.2. Analysis of the Influence of DFIM Parameters on Control Characteristics

3.2.1. Inductance and Resistance of DFIM. The inductance and resistance are related to the design of the DFIM. In this paper, according to the characteristics that the DFIM design should satisfy, the inductance and resistance of the DFIM are taken as follows through electromagnetic design (relevant parameters are converted to the two-phase rotating coordinate system by Parker transformation). Stator side resistance R_s, 0.00103 Ω; stator side leakage inductance L_s, 0.000194 H; rotor side resistance R_r, 0.000650 Ω; rotor side leakage inductance L_r, 0.000267 H; excitation inductance L_m, 0.00567 H.

3.2.2. Flywheel Torque GD^2. Flywheel torque is the product of the weight of the rotating part of the generator and the square of its inertia diameter. GD^2 indicates the ability of the rotating part of the unit to maintain the original motion state when there is a large disturbance in the power system, which directly affects the speed increase rate of the generator during load rejection and the operation stability of the generator when the system load changes suddenly. It also has a great impact on the transient process and dynamic stability of the power system. The larger the GD^2, the smaller the unit speed change rate and the higher the system stability. However, when the GD^2 is too large, the unit weight increases and the cost increases.

Figure 10 shows the impact of the rotary inertia on the speed increase during load shedding when other parameters are unchanged.

Figure 11 shows the variation of the pole-zero diagram of the speed closed-loop transfer function when the rotary inertia J of the unit changes. It can be found that when the rotary inertia is small, the conjugate pole is located in the right half-plane and the speed closed-loop is unstable. As the rotary inertia increases, the conjugate pole transitions to the left half-plane and the speed closed-loop is stable. So we take the intermediate value of the value range of J in Figure 10, $J = 4{,}000{,}000\ \text{kg m}^2$ in this paper.

In this paper, other parameters of the unit are selected as follows. Rated power, 300 MW; rated voltage, 18 kV; rated frequency, 50 Hz; pole pair number, 12; and friction factor B_m is ignored.

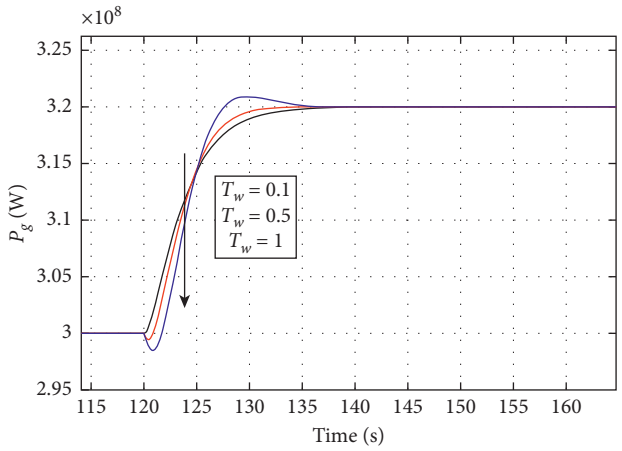

Figure 9: The influence of parameter T_w on the output power of the unit to the power grid.

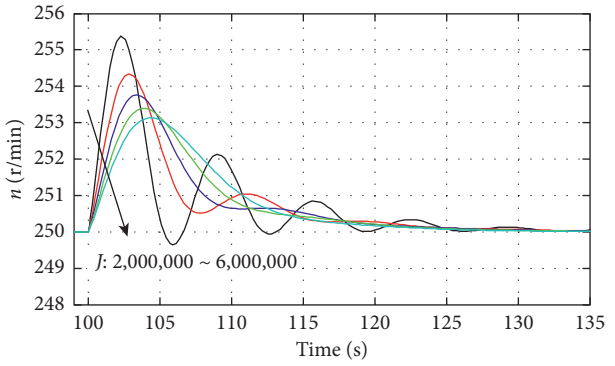

Figure 10: Effect of rotary inertia on Speed Response.

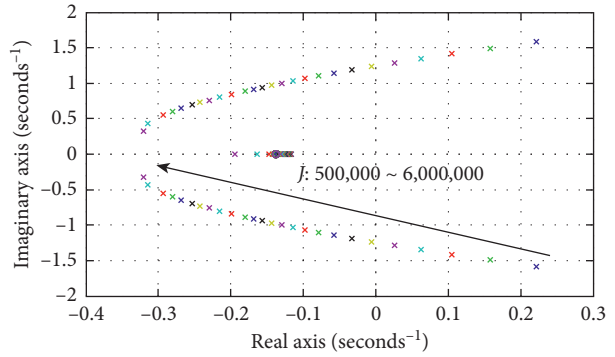

Figure 11: Change of zero-pole diagram of speed closed-loop transfer function when J of unit changes.

4. Control Parameter Design of the Unit Control System

After the parameters of the pump turbine and DFIM are given, the control characteristics of the unit are directly related to the parameters in different control strategies. Therefore, control parameters in different strategies need to be designed to achieve the optimal effect, including the control parameters of the pump turbine adjustment system and the excitation system. The general method to design parameters of the control system is as follows.

(1) Determine the value range of the parameters in the control system for the stability of the system;

(2) Determine the steady-state error of the system and further determine the value range of the parameters of the control system (The main discussion is the steady-state error of the system with the unit step input $R(s) = 1/s$);

(3) Determine the parameters based on the response of the control system to the step input signal (Select the parameter with the best effect according to the overshoot amount and adjustment time of the output waveform of the control system).

4.1. Control Parameters Design in the Generating Mode

4.1.1. Power Priority Control Strategy. The control block diagram when the power priority control strategy is adopted in the generating mode is shown in Figure 8. Among them, standard values are used when the pump turbine regulating system is involved in calculation, and the actual value is used in the rest part. P_{base} and n_{base} are the reference values of power and speed, respectively, and their values take the rated values. The control parameters include the parameters of the DFIM excitation system and the pump-turbine adjustment system. By observing the block diagram, it can be found that the power control closed loop is a separate closed loop, which has nothing to do with the speed closed loop. The speed control closed loop is coupled with the power closed loop, which is affected by the power closed loop.

(1) Control Parameters Design for DFIM Excitation Control System. The power control closed loop is shown in Figure 12.

Let $k_2 = -3U_sL_m/2L_s$, then the open-loop transfer function of the power control closed-loop is shown in the following formula:

$$G_0(s) = -k_2 \frac{k_{\text{PWM}}}{T_s s + 1} \cdot \frac{k_{p_1} s + k_{i_1}}{s}. \tag{9}$$

Closed-loop transfer function is shown in the following formula:

$$G_c(s) = \frac{-k_2 k_{\text{PWM}} \left(k_{p_1} s + k_{i_1}\right)}{s\left(T_s s + 1\right) - k_2 k_{\text{PWM}} \left(k_{p_1} s + k_{i_1}\right)}. \tag{10}$$

(i) Stability of Control Closed-Loop. According to the open-loop transfer function of the active power control closed loop, this closed loop has a pole located at the origin. The closed-loop transfer function is used to determine the stability. The pole discriminant of the closed-loop transfer function is shown in the following formula:

$$s\left(T_s s + 1\right) - k_2 k_{\text{PWM}} \left(k_{p_1} s + k_{i_1}\right) = 0. \tag{11}$$

Generally, the switching frequency of the PWM link is 2 kHz–10 kHz, so the effect of the time constant T_s can be

ignored. It can be obtained that the parameter value range of making the control closed-loop stable is shown in the following formula:

$$\frac{-k_2 k_{\mathrm{PWM}} k_{i_1}}{1 - k_2 k_{\mathrm{PWM}} k_{p_1}} \geq 0. \tag{12}$$

When PI parameters are not less than zero, the active power control closed-loop is stable.

(ii) Steady-State Characteristics of the Control Closed-Loop

$$K_p = \lim_{s \longrightarrow 0} G_0(s) = -k_2 k_{\mathrm{PWM}} \lim_{s \longrightarrow 0} \left(k_{p_1} + \frac{k_{i_1}}{s} \right). \tag{13}$$

When k_{p_2} is not zero and k_{i_2} is not zero, the system is a no-deviation adjustment.

(iii) Step Signal Response of the Control Closed-Loop. According to References [32] and [33], large pumped storage units are required to have the ability to increase or decrease the load by 10 MW per second. Therefore, the design of the PI regulator parameters of the excitation system should be able to track the change of the command value within about 1s, and the overshoot is relatively small. According to the regulation of response time, when $k_{p_1} = 0.00005$ and $k_{i_1} = 0.0005$, the active power control closed-loop has a better response characteristic to the step signal, and its response waveform is shown in Figure 13.

(2) Control Parameters Design for the Pump Turbine Adjustment System. The pump turbine adjustment system is located in the speed control closed-loop. Therefore, the design of its parameters needs to analyze the speed control closed-loop. At this time, the power control closed-loop is a disturbance in the speed control closed-loop. The linearized block diagram of the speed control closed-loop is shown in Figure 14.Also,

$$G_{\mathrm{Te}}(s) = \frac{\Delta T_e}{\Delta P_{\mathrm{sref}}} = -\frac{3\omega_s p_n U_s L_m}{2L_s\left(s^2 + \omega_s^2\right)} \cdot \frac{-\left(k_{p_1} s + k_{i_1}\right) k_{\mathrm{PWM}}}{s\left(T_s s + 1\right) - k_2\left(k_{p_1} s + k_{i_1}\right) k_{\mathrm{PWM}}}. \tag{14}$$

Open-loop transfer function of the speed control closed-loop is shown in the following formula:

$$G_0(s) = \frac{P_{\mathrm{base}}}{\omega_{r_0}\omega_{\mathrm{base}}} \cdot \frac{1 - T_w s}{\left(0.07s^2 + s + 1\right)\left(1 + 0.5T_w s\right)} \cdot \frac{\omega_{r_0}^2}{\omega_{r_0}^2 (Js + B) + P_{m_0}} \cdot \left(k_{p_2} + \frac{k_{i_2}}{s} \right). \tag{15}$$

Closed-loop transfer function of the speed control closed-loop is shown in the following formula:

$$G_C(s) = \frac{\left(P_{\mathrm{base}}/\omega_{r_0}\omega_{\mathrm{base}}\right) \cdot \left(1 - T_W s\right) \cdot \left(k_{p_2} s + k_{i_2}\right)}{s\left(0.07s^2 + s + 1\right)\left(1 + 0.5T_W s\right)\left(Js + B + \left(P_{m_0}/\omega_{r_0}^2\right)\right) + \left(P_{\mathrm{base}}/\omega_{r_0}\omega_{\mathrm{base}}\right) \cdot \left(1 - T_W s\right) \cdot \left(k_{p_2} s + k_{i_2}\right)}. \tag{16}$$

The active power control closed-loop is used as disturbance input to the speed control closed-loop. The closed-loop transfer function of the disturbance is shown in the following formula:

$$G_D(s) = \frac{G_{T_e}(s) \cdot s\left(0.07s^2 + s + 1\right)\left(1 + 0.5T_W s\right)}{s\left(0.07s^2 + s + 1\right)\left(1 + 0.5T_W s\right)\left(Js + B + \left(P_{m_0}/\omega_{r_0}^2\right)\right) + \left(P_{\mathrm{base}}/\omega_{r_0}\omega_{\mathrm{base}}\right) \cdot \left(1 - T_W s\right) \cdot \left(k_{p_2} s + k_{i_2}\right)}. \tag{17}$$

(i) Stability of the Speed Control Closed-Loop. The open-loop transfer function and the closed-loop transfer function of the speed control closed-loop are shown in formulas (15) and (16). It can be seen that the transfer function of the speed control closed-loop is very complex, and its characteristic equation is a five-order function, as shown in formula (18). It is difficult to directly obtain the range of control parameters that meet the stability requirements. Therefore, the influence of the control parameters on the zero-pole diagram of the closed-loop transfer function is firstly analyzed, and the

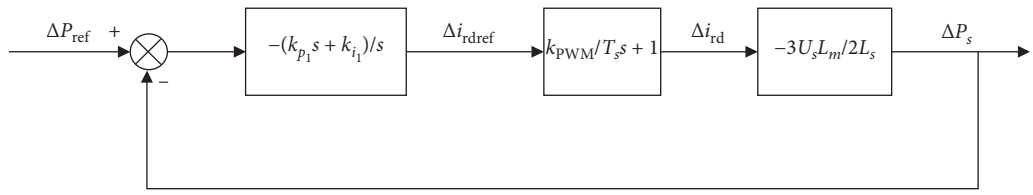

Figure 12: Power control closed loop.

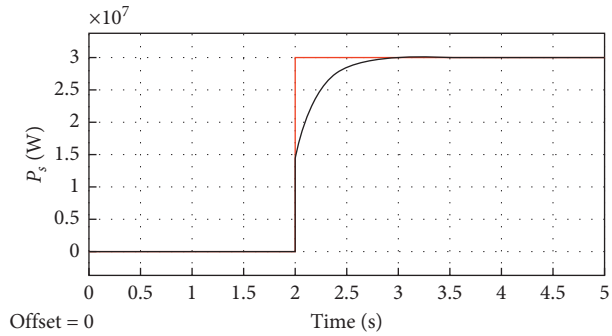

Figure 13: Response waveform of the active power control closed-loop to the step signal.

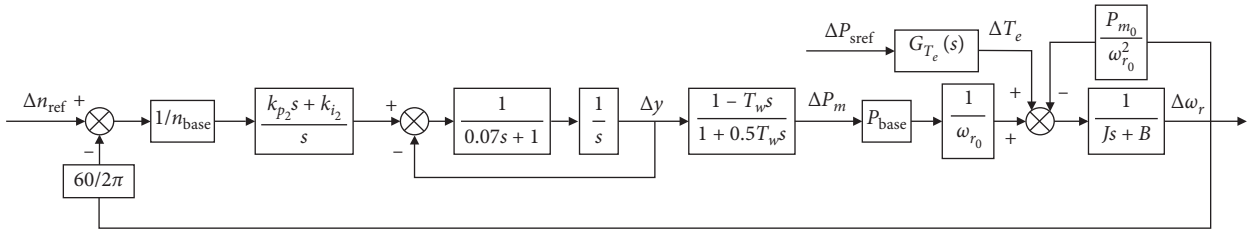

Figure 14: Linearized block diagram of the speed control closed-loop.

influence law between the control parameters and the stability of the control closed-loop is summarized. Then, the value range of the control parameters is approximately determined. The analysis is as follows:

$$s\left(0.07s^2 + s + 1\right)\left(1 + 0.5T_w s\right)\left(Js + B + \frac{P_{m_0}}{\omega_{r_0}^2}\right) + \frac{P_{\text{base}}}{\omega_{\text{base}}\omega_{r_0}}\left(1 - T_w s\right)\left(k_{p_2}s + k_{i_2}\right) = 0. \tag{18}$$

Figure 15 shows the change of the zero-pole diagram of the closed-loop transfer function when k_{p_2} changes but k_{i_2} remains unchanged. When k_{p_2} increases, there is a zero point in the right-half plane of the closed-loop transfer function, so the response of speed control closed-loop will have a negative adjustment. The poles of the right half plane change from a pair of conjugate poles to no right half plane poles and then to a pair of right half plane poles. Therefore, when the k_{i_2} is unchanged and k_{p_2} takes a certain value in the middle, the closed-loop speed will be stable. In other words, beyond this range, it will be unstable.

Figure 16 shows the change of the zero-pole diagram of the closed-loop transfer function when k_{i_2} changes and k_{p_2} remains unchanged. Similar to the change of k_{p_2}, there is a zero point in the right half plane in this case, and k_{i_2} does not affect the position of the zero point. For convenience of observation, the zero point is not considered, the poles far from the right half plane are also not considered, and only the influence of k_{i_2} on the position of the conjugate pole is considered. Through observation, when other parameters are unchanged, and k_{i_2} gradually increases, the conjugate pole gradually enters the right half plane. So, when k_{i_2} is less than a certain value, the speed control closed-loop is stable.

According to the above rules about the influence of control parameters on stability and the response of the speed control closed-loop to the step signal, the approximate range of control parameters that meet the stability requirements is given, as shown in the shaded part of Figure 17.

(ii) Steady-State Characteristics of the Speed Control Closed-Loop. The steady-state error of speed control closed-loop with step input is shown in the following formula:

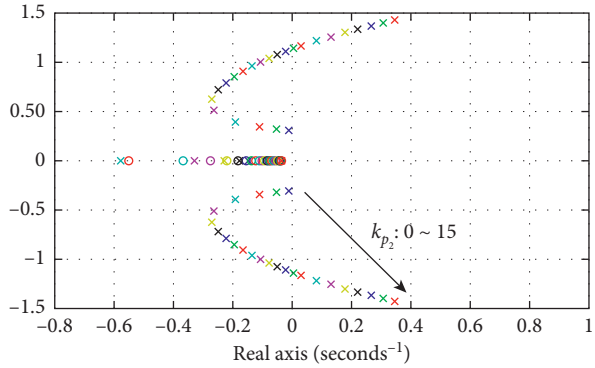

Figure 15: The change of the zero-pole diagram of the speed control closed-loop when the k_{p_2} changes.

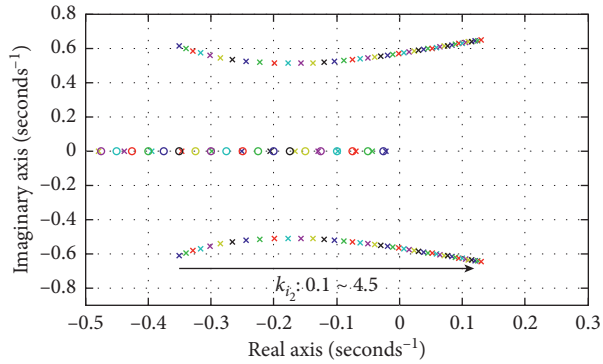

Figure 16: The change of the zero-pole diagram of the speed control closed-loop when the k_{i_2} changes.

$$K_p = \lim_{s \longrightarrow 0} G_0(s) = \lim_{s \longrightarrow 0} \left(k_{p_2} + \frac{k_{i_2}}{s} \right). \tag{19}$$

It can be obtained that when parameter k_{i_2} is not zero, the system can realize a no-deviation adjustment for the step input.

The effect of the active power control closed-loop on steady-state error can be expressed by the following formula:

$$y_D(\infty) = \frac{-k_2 k_{\mathrm{PWM}} \left(k_{p_1} + \left(k_{i_1}/s \right) \right)}{1 - k_2 k_{\mathrm{PWM}} \left(k_{p_2} + \left(k_{i_1}/s \right) \right)} \cdot \frac{-\left(3 p_n U_s L_m / 2 \omega_s L_s \right) \cdot \left(\omega_{r_0}^2 / \left(\omega_{r_0}^2 B + P_{m_0} \right) \right)}{1 + \left(\omega_{r_0}^2 / \left(\omega_{r_0}^2 B + P_{m_0} \right) \right) \cdot \left(P_{\mathrm{base}} / \omega_{r_0} \omega_{\mathrm{base}} \right) \cdot \left(k_{p_2} + \left(k_{i_2}/s \right) \right)}. \tag{20}$$

When k_{i_1} and k_{i_2} are not equal to zero, the adjustment of the system is a no-deviation adjustment. Therefore, considering the abovementioned effects on the steady-state error of the system, the parameter k_{i_2} cannot be set to zero.

(iii) Step Signal Response of the Speed Control Closed-Loop. The requirement of the pump turbine regulation system of the speed control closed-loop on the response of step signal generally requires that the speed control closed-loop can track the speed instruction, achieve stability within 20 seconds or so, and the overshoot should not be too large.

(a) Analysis of the Influence of the Control Parameters on the Overshoot and the Adjustment Time When the Speed Is Adjusted, . The change of overshoot and adjustment time with different k_{p_2} and k_{i_2} are shown in Figure 18. Judging from the two figures, it can be found that the overshoot does not decrease when the k_{p_2} increases, and the adjustment time does not decrease when the k_{i_2} increases. The transfer function has a pair of conjugate poles. When the parameters k_{p_2} and k_{i_2} increase, the fluctuations increase, which will increase the overshoot and the adjustment time. Therefore, selecting parameters k_{p_2} and k_{i_2} within a reasonable range will make the overshoot and adjustment time smaller.

According to the setting requirements for adjustment time and overshoot, $k_{p_2} = 3$ and $k_{i_2} = 0.55$ are a set of reasonable values. At this time, the step signal response and the Bode diagram of the open-loop transfer function are shown in Figure 19. Observing the Bode diagram, the phase margin is between 40 and 50°, and the amplitude margin is about 10.

(b) Analysis of the Magnitude of the Speed Fluctuation Caused by the Adjustment of the Power Control Closed-Loop When the Speed Is Not Adjusted. Figure 20 shows the

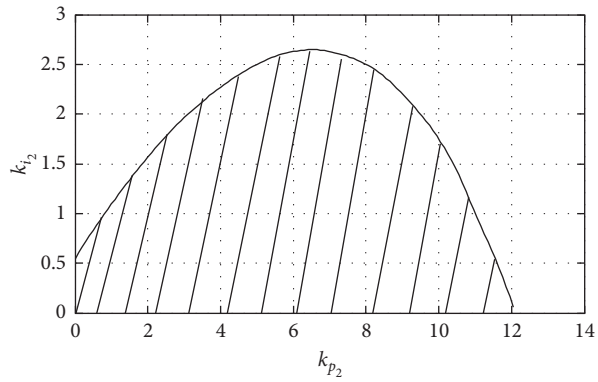

Figure 17: Value range of k_{p_2} and k_{i_2} that meet stability.

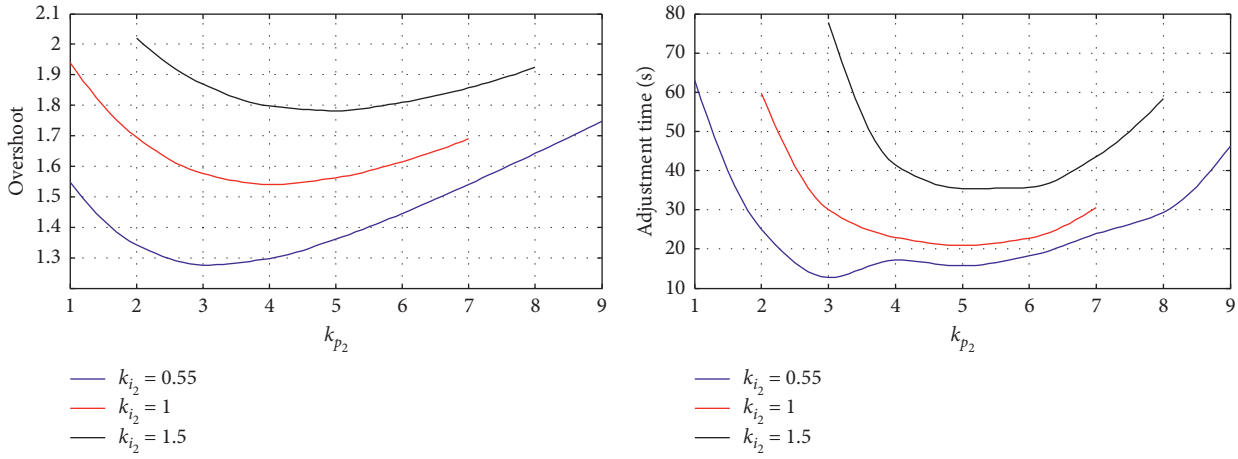

(a) (b)

Figure 18: Influence of the k_{p_2} and k_{i_2} on the overshoot and adjustment time..

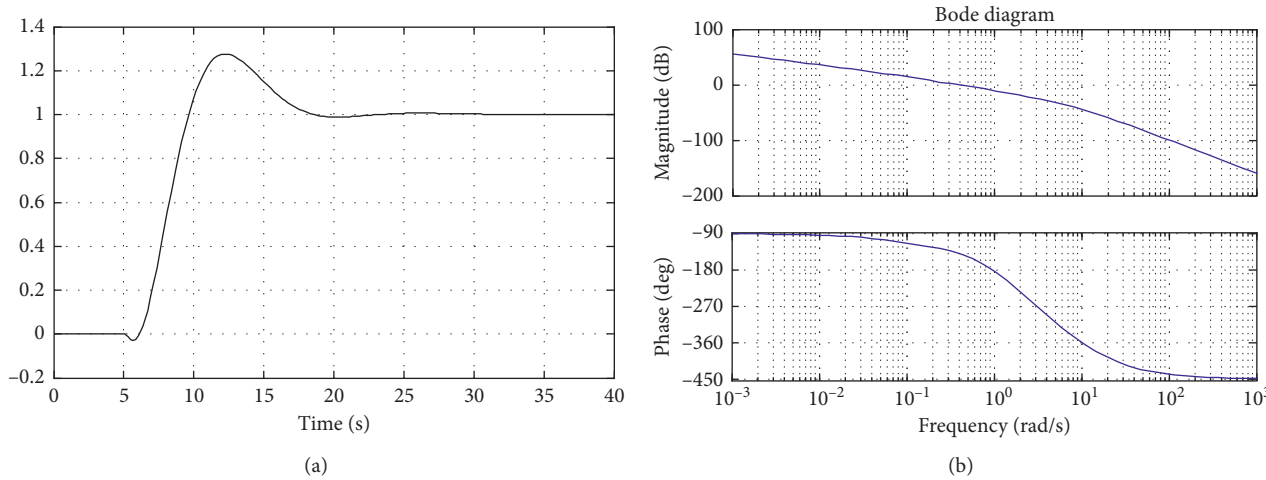

(a) (b)

Figure 19: Time domain response and Bode diagram of control closed-loop with $k_{p_2} = 3$, $k_{i_2} = 0.55$. (a) Time domain response of the step signal. (b) Bode diagram of the open-loop transfer function.

magnitude of the speed fluctuation caused by different response times when adjusting the stator-side power of different sizes. It can be found that the greater the power change, the greater the speed fluctuation; the shorter the response time of the stator side power, the greater the speed fluctuation.

Figure 21 shows that the maximum speed fluctuation caused by the stator-side power adjustment when k_{p_2} changes to k_{i_2} remains unchanged. It can be found that the larger the parameter k_{p_2}, the better the suppression effect on the speed fluctuation caused by the stator side power adjustment; the larger the amount of power adjusted on the stator side, the greater the fluctuation of the speed.

In summary, when the speed is adjusted, the optimal PI parameters are $k_{p_2} = 3$ and $k_{i_2} = 0.55$; when keeping the speed command unchanged, considering the speed fluctuation caused by the power adjustment on the stator side, it is found that the larger the parameter k_{p_2}, the better the suppression effect. Therefore, we need to make a compromise, taking $k_{p_2} = 4$ and $k_{i_2} = 0.55$.

4.1.2. Speed Priority Control Strategy. Figure 7 shows the overall structure when the speed priority control strategy is adopted in the generating mode. Combined with the mathematical model of each part of the DFVSPS unit, the overall structure of the DFVSPS unit with speed priority control strategy can be simplified into the control block diagram shown in Figure 22.

When the speed priority control strategy is adopted in the generating mode, the control parameter design method is the same as that in the power priority control strategy. In this paper, the analysis results are given directly without further details.

The block diagram of the control closed loop (i.e., mechanical power control closed loop) where the pump turbine control system is located is shown in Figure 23.

The open-loop and closed-loop transfer function of the mechanical power control closed-loop are shown in

$$G_0(s) = \frac{k_{p_2}s + k_{i_2}}{s} \cdot \frac{1}{0.07s^2 + s + 1} \cdot \frac{1 - T_w s}{1 + 0.5T_w s}, \tag{21}$$

$$G_c(s) = \frac{\left(k_{p_2}s + k_{i_2}\right)\left(1 - T_w s\right)}{s\left(0.07s^2 + s + 1\right)\left(1 + 0.5T_w s\right) - \left(k_{p_2}s + k_{i_2}\right)\left(1 - T_w s\right)}. \tag{22}$$

The control parameters k_{p_2} and k_{i_2} that make the mechanical power control closed-loop stable are obtained in the same way as the power priority control strategy, as shown in Figure 24.

Among them, when the control parameters k_{p_2} and k_{i_2} do not take zero, the mechanical power control closed loop is a no-deviation adjustment.

The linearized block diagram of the excitation system control closed-loop (i.e., speed control closed-loop) is shown in Figure 25.

The open-loop transfer function, closed-loop transfer function, and the transfer function of the disturbance to the output of the speed control closed-loop are shown in formulas (23)–(25). Where, $G_{\mathrm{Pm}}(s)$ is the closed-loop transfer function of the mechanical power control closed-loop.

$$G_0(s) = \frac{60}{2\pi} \cdot \frac{k_{p_1}s + k_{i_1}}{s} \cdot \frac{k_{\mathrm{PWM}}}{T_s s + 1} \cdot \frac{3\omega_s p_n L_m U_s}{2L_s\left(s^2 + \omega_s^2\right)} \cdot \frac{\omega_{r_0}^2}{\omega_{r_0}^2\left(Js + B\right) + P_{m_0}}, \tag{23}$$

$$G_c(s) = \frac{(60/2\pi) \cdot \left(k_{p_1}s + k_{i_1}\right) \cdot \left(k_{\mathrm{PWM}}/\left(T_s s + 1\right)\right) \cdot \left(3\omega_s p_n L_m U_s/2L_s\left(s^2 + \omega_s^2\right)\right)}{s\left(Js + B + \left(P_{m_0}/\omega_{r_0}^2\right)\right)\left(T_s s + 1\right) + (60/2\pi) \cdot k_{\mathrm{PWM}} \cdot \left(k_{p_1}s + k_{i_1}\right) \cdot \left(3\omega_s p_n L_m U_s/2L_s\left(s^2 + \omega_s^2\right)\right)}, \tag{24}$$

$$G_D(s) = \frac{G_{P_m}(s)}{\omega_{r_0}} \cdot \frac{s\left(T_s s + 1\right)}{s\left(Js + B + \left(P_{m_0}/\omega_{r_0}^2\right)\right)\left(T_s s + 1\right) + (60/2\pi) \cdot k_{\mathrm{PWM}} \cdot \left(k_{p_1}s + k_{i_1}\right) \cdot \left(3\omega_s p_n L_m U_s/2L_s\left(s^2 + \omega_s^2\right)\right)}. \tag{25}$$

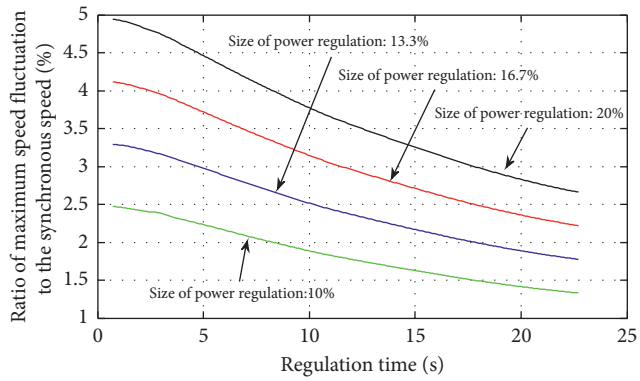

Figure 20: Effect of the power control closed-loop response time on the speed.

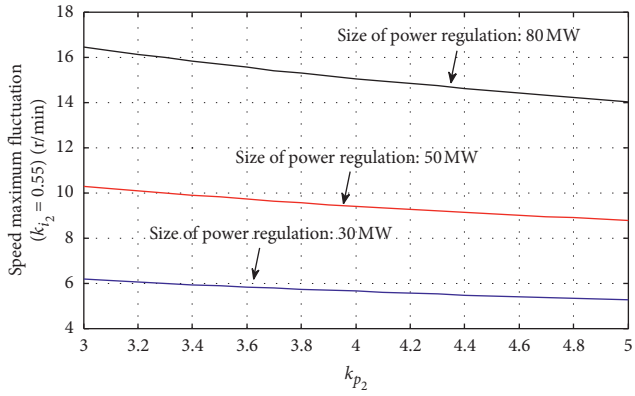

Figure 21: Speed fluctuation caused by the stator side power adjustment with different k_{p_2}.

Same as the power priority control strategy, ignoring the effects of the PWM link and nondominant poles caused by changes of the magnetic flux, the values of the control parameters k_{p_1} and k_{i_1} that stabilize the excitation system are shown in formula (26). Here, $k_1 = 3p_nL_mU_s/2L_s\omega_s$.

$$\begin{cases} k_{p_1} > \dfrac{\left(P_{m_0}/\omega_{r_0}^2\right) + B}{9.55k_1}, \\ k_{i_1} > 0. \end{cases} \tag{26}$$

Among them, when the parameter k_{i_1} is not zero, the control closed-loop is a no-deviation adjustment, and the disturbance amount has no effect on the closed-loop after stabilization.

By analyzing the step signal response of two control closed-loop, it is concluded that $k_{p_1} = 400$, $k_{i_1} = 50$, $k_{p_2} = 0.1$, $k_{i_2} = 0.25$ are a set of ideal control parameters.

4.2. Control Parameters Design in the Pump Mode. With reference to the design of the control parameters of the two control strategies in the generating mode, the control parameters of the two control strategies in the pump mode are designed. Different from the generating mode, when it is in the pump mode, the change of the guide vane opening of the unit has no obvious regulating effect on the unit power when operating near the rated operating point, while the unit speed has a clear regulation effect on the output power of the pump turbine. According to the actual unit operation data, the absorbed power of the pump turbine is proportional to the cube of speed. Therefore, the guide vane opening adjustment system of the pump turbine loses its adjustment function when it is operated near the rated working condition. In fact, only the excitation control system plays an adjustment role in the entire control system.

4.2.1. Power Priority Control Strategy. The block diagram of the power priority control strategy in the pump mode is shown in Figure 26.

At this time, the control closed loop where the excitation control system is located is the active power closed loop, and its block diagram is shown in Figure 27.

It can be seen that the active power control closed-loop is exactly the same as the power control closed-loop when the power priority control strategy is used in the generating mode, but it is not repeated here. The conclusion is that the value range of the control parameter PI1 is k_{p_1}, 0.00005–0.0005; k_{i_1}, 0.0005–0.005. The control effect is shown in Figure 28.

4.2.2. Speed Priority Control Strategy. The block diagram of speed priority control strategy in the pump mode is shown in Figure 29.

The control closed loop where the excitation control system is located is the speed control closed loop when the speed priority control strategy is adopted for the pump mode. The block diagram of the speed control closed-loop after linearization is shown in Figure 30.

Where, parameter k_3 can be expressed as the following formula:

$$k_3 = P_{\text{base}}\left(\frac{60}{2\pi} \cdot \frac{1}{n_{\text{base}}}\right)^3. \tag{27}$$

Open-loop and closed-loop transfer function of the speed control closed-loop are shown in:

$$G_0(s) = \frac{60}{2\pi} \cdot \frac{k_{\mathrm{PWM}}}{T_s s + 1} \cdot \frac{3\omega_s p_n L_m U_s}{2L_s\left(s^2 + \omega_s^2\right)} \cdot \frac{k_{p_1} s + k_{i_1}}{s} \cdot \frac{1}{Js + B + 2k_3\omega_{r_0}}, \tag{28}$$

$$G_C(s) = \frac{(60/2\pi) \cdot k_{\mathrm{PWM}} \cdot \left(3\omega_s p_n L_m U_s / 2L_s\left(s^2 + \omega_s^2\right)\right) \cdot \left(k_{p_1} s + k_{i_1}\right)}{s\left(Js + B + 2k_3\omega_{r_0}\right)\left(T_s s + 1\right) - (60/2\pi) \cdot k_{\mathrm{PWM}} \cdot \left(3\omega_s p_n L_m U_s / 2L_s\left(s^2 + \omega_s^2\right)\right) \cdot \left(k_{p_1} s + k_{i_1}\right)}. \tag{29}$$

It is the same as the analysis method of the speed priority control strategy in the generating mode. The effects of PWM links and nondominant poles caused by changes in the magnetic flux are not considered. After calculation, the range of k_{p_1} that meets the stability requirement is shown in the following formula:

$$k_{p_1} > \frac{B + 2k_3\omega_{r_0}}{9.55k_2}. \tag{30}$$

Since the coefficient k_2 is less than zero and the coefficient k_3 is greater than zero, the speed control closed loop is stable in the condition of $k_{p_1} > 0$, and the speed control closed loop can realize the no-deviation adjustment in the condition of $k_{i_1} > 0$.

After the response of the closed loop to the step signal is analyzed, when $k_{p_1} = 100$ and $k_{i_1} = 50$, the speed control closed-loop has good control characteristics.

5. Comparison of Unit Control Characteristics

5.1. Comparison of Control Characteristics of Two Control Strategies in the Generating Mode. In the previous section, the control characteristics of a DFVSPS unit in the generating mode when the power priority control strategy and the speed priority control strategy are adopted are analyzed. In the generating mode, different control strategies are adopted, which have different control characteristics. Therefore, a comparative analysis of the characteristics of the two control strategies is needed to obtain the applicable working conditions of different control strategies.

5.1.1. When the Speed Is Not Adjusted, Only the Output Active Power Is Adjusted. Suppose that the unit is at rated operation in the generating mode before adjustment (P = 300 MW, n = 250 r/min), keep the speed command unchanged, reduce active power by 30 MW at t = 120 s, and increase active power by 30 MW at t = 200 s. The positive direction of active power is from the DFVSPS unit to the power grid. At this time, the relative waveforms of the two control strategies are compared as shown in Figures 31 and 32.

The speed comparison diagram of two control strategies in the generating mode when n_{ref} is unchanged and P_{ref} is changed is shown in Figure 31, and the actual dynamic responses for a DFVSPS unit when using the power priority control strategy in the generating mode are available in [23, 32]. When the power priority control strategy is adopted, the active power is controlled by the DFIM excitation system. When the power reference value is reduced, the d-axis current which controls the active power is reduced. Since the electromagnetic torque is also controlled by the d-axis current, it is also reduced; during the generating mode, the DFIM is dragged by the pump turbine. When the active power adjustment occurs, the mechanical torque does not change, and the decrease of the electromagnetic torque causes the unit speed increase, which returns to the command value because of the speed control closed loop. In the speed priority control strategy, the active power is controlled by the pump turbine adjustment system. When the power reference value is reduced, the mechanical torque is reduced. At this time, the electromagnetic torque does not change, and the unit speed is reduced. When the power reference value increases, the speed with the power priority control strategy will first decrease and then return to the command value; the speed of applying the speed priority control strategy first increases and then returns to the command value.

The comparison diagram of the stator-side active power is shown in Figure 32(a). Applying the power priority control strategy, the stator-side active power can quickly track the change of the command and respond in about 1 s; while applying the speed priority control strategy, the change of the power reference causes the adjustment of the guide vane opening of the pump turbine, and then changes the output mechanical power of the pump turbine. When the shaft torque is unbalanced, the rotation speed is changed. Then, the adjustment of the DFIM excitation system is triggered, and the stator-side power is adjusted accordingly. The whole process is accompanied by hydraulic adjustment and mechanical adjustment. The inertia time constant is large, the response time is long, and the power adjustment takes tens of seconds.

The comparison diagram of mechanical power is shown in Figure 32(b). The adjustment of mechanical power is related to the speed change. Applying the power priority control strategy, compared with the speed priority control strategy, the power response is faster, causing a larger change in torque, and a larger amount of torque imbalance on the shaft in a short period of time. Therefore, there are larger fluctuations in speed and mechanical power.

By comparison, when power control is carried out, the power priority control strategy can achieve a response within

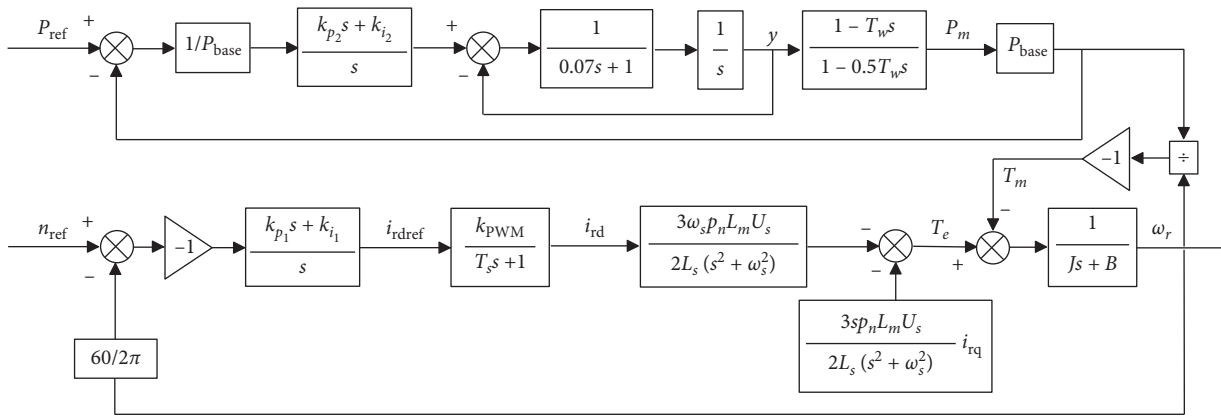

Figure 22: Control block diagram of the speed priority control strategy in the generating mode.

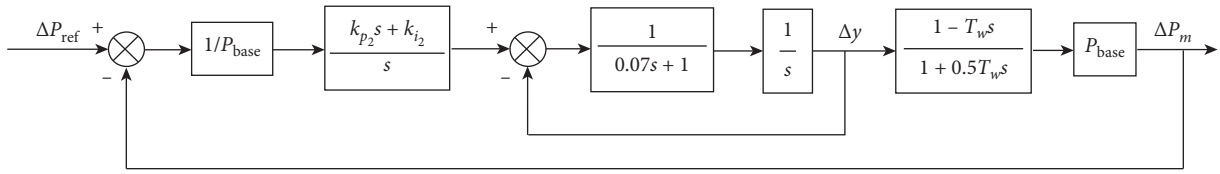

Figure 23: Control block diagram of the mechanical power control closed-loop.

milliseconds, while the speed priority control strategy cannot achieve such a fast response due to the constraints of water flow inertia and rotating shaft inertia of the unit. Regarding the speed fluctuation caused by the two control strategies, it is related to the power response time. The power priority control strategy causes larger speed fluctuation due to its extremely fast adjustment. According to the foregoing analysis, when the power response time of the power priority control strategy is equivalent to the speed priority control strategy, the speed fluctuations caused are also equivalent.

5.1.2. When the Active Power Is Not Adjusted, Only the Speed Is Adjusted. Suppose that the unit operates at rated condition in the generating mode before adjustment (P = 300 MW, n = 250 r/min). Keep P_{ref} unchanged, n_{ref} decrease by 5 r/min at t = 120 s, and increase by 5 r/min at t = 200 s. At this time, the comparison of related waveform diagrams in the two strategies is shown in Figures 33 and 34.

Observing Figure 33, it can be found that when the speed priority control strategy is adopted, the speed can reach stability faster, and the power priority control strategy requires longer adjustment time. Because of applying the power priority control strategy, the speed must be adjusted by the pump turbine, and the water inertia affects the speed of speed adjustment. Observing Figure 34, the impact of speed adjustment on power is as follows. When the power priority control strategy is used, the stator-side active power control closed loop is an independent control closed loop and is not affected by the speed adjustment. Therefore, when the speed is adjusted, the stator-side power remains unchanged, while the guide vane opening changes with the adjustment of the speed, and the mechanical power changes accordingly; when the speed priority control strategy is adopted, the mechanical power control closed-loop is an independent closed-loop, which is not affected by the speed control closed-loop. Therefore, during the speed adjustment process, the mechanical power remains unchanged, while the stator current and rotor current of the DFIM changes due to the speed adjustment, and the stator-side power changes.

5.1.3. When the Active Power and Speed Need to Be Adjusted at the Same Time. Suppose that the unit operates at rated condition in the generating mode before adjustment (P = 300 MW, n = 250 r/min). When the power and speed need to be adjusted at the same time, the power is reduced by 30 MW at t = 120 s, and the speed reference value is reduced by 5 r/min. At t = 200 s, the power is increased by 30 MW, and the speed reference value is increased by 5 r/min. At this time, the comparison of related waveform diagrams in the two control strategies is shown in Figures 35 and 36.

For the power priority control strategy, due to its ms-level power adjustment capability, the power adjustment has been completed at the beginning of the speed adjustment, so the torque imbalance caused by the power adjustment will make the speed increase first, and then reduce to the command value due to the function of speed control closed-loop. And, the adjustment of mechanical power is accompanied by the entire speed adjustment process; regarding the speed priority control strategy, the power and the speed adjustment process are performed simultaneously. Because the reduction of power will cause the speed to decrease, the two processes are in the same direction. At the same time, due to the sudden

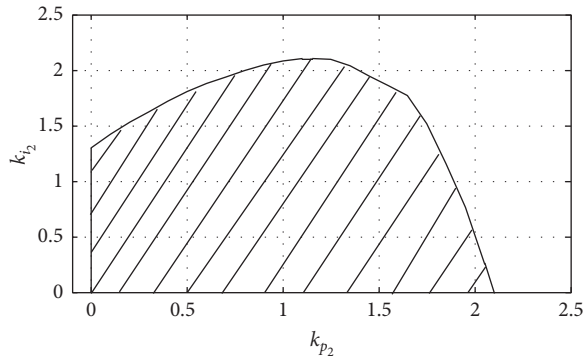

Figure 24: Value range of control parameters k_{p_2} and k_{i_2}.

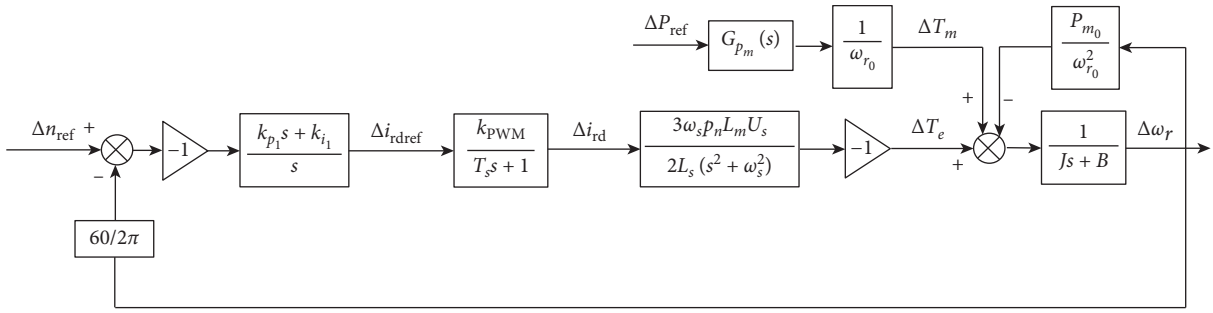

Figure 25: Control block diagram of the speed control closed-loop.

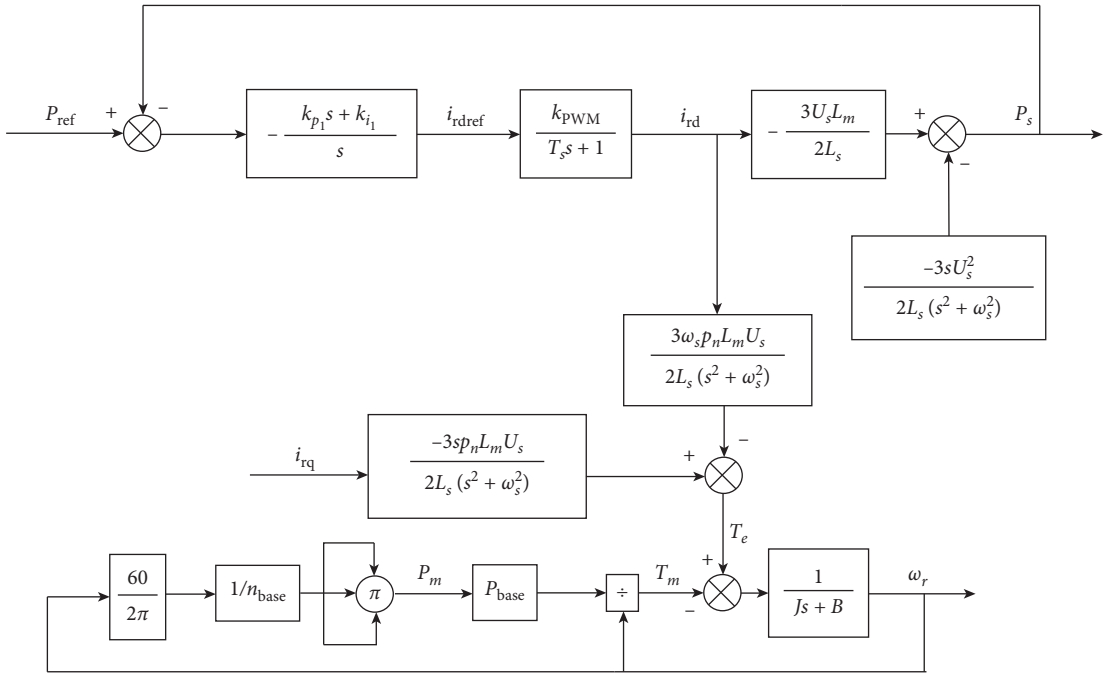

Figure 26: Control block diagram of the power priority control strategy in the pump mode.

change of the speed command, the speed error is amplified by the PI regulator and input to the DFIM, which will cause a sudden change of the stator-side power.

In this case, the speed priority control strategy has no obvious advantages compared with the power priority control strategy in speed control. In terms of power control, the response time is long, the power fluctuation is large, and the effect is not as good as the power priority control strategy. Therefore, the power priority control strategy should be adopted in this case.

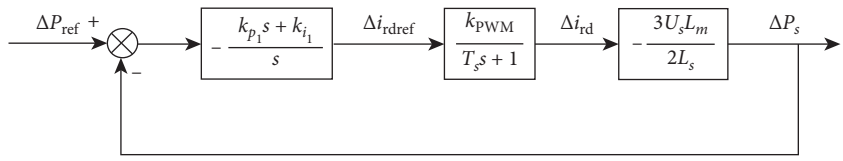

Figure 27: Active power control closed-loop.

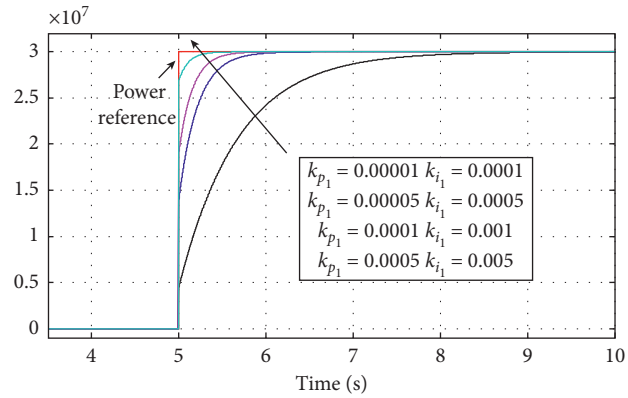

Figure 28: Time domain response of the active power control closed-loop to the step signal with different k_{p_1} and k_{i_1}.

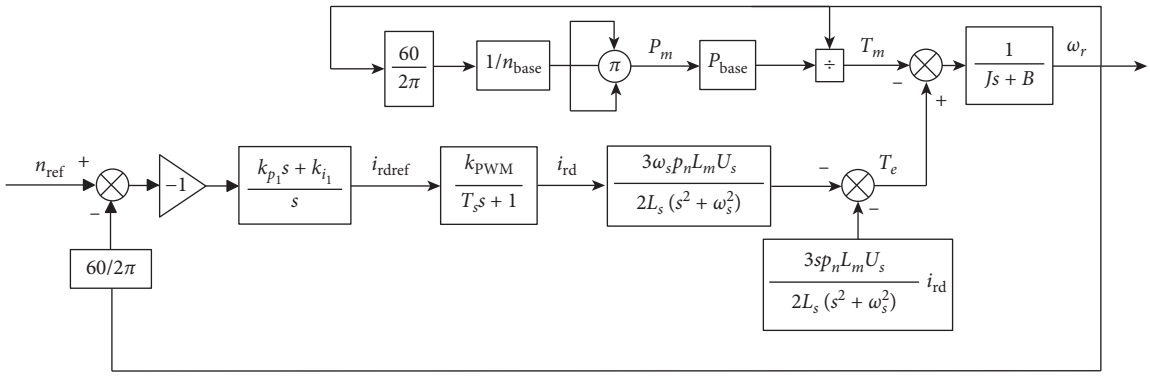

Figure 29: Block diagram of the speed priority control strategy in the pump mode.

5.2. Comparison of Control Characteristics of Two Control Strategies in Pump Mode. We analyze the control characteristics of the two strategies when the unit is operating in pump mode. Same as the generating mode, the control characteristics of the two control methods need to be compared to obtain the applicable conditions for different methods. According to the control parameters designed above, the relevant waveform diagrams are shown in Figures 37–39. The actual dynamic responses for a DFVSPS unit using power priority control strategy in the pump mode are available in [23, 32]. The positive direction of active power in the pump mode is from the power grid to the unit.

Comparing the two control strategies in the pump mode; although the controlled objects of the two control strategies are different, the characteristics of the control strategy can be judged by the response to the step signal. Due to the unit's moment of inertia, the response time of the speed is relatively long in the two control strategies. The speed priority control strategy can shorten the speed response time, but the effect is not obvious. As for the stator-side active power, when the pow`er priority control strategy is used, the power can be adjusted in milliseconds and the waveform is stable; while the speed priority control strategy is constantly adjusting the stator current due to the long-term adjustment of the speed, the stator-side power adjustment time is also very long, the waveform is not good, and the grid-connected power fluctuates greatly. The mechanical power waveform of the pump turbine is similar to the waveform of the speed because it is proportional to the cube of the rotation speed, so it will not be repeated here.

Based on the above comparison, combined with the operating characteristics of DFVSPS units, the main purpose of achieving variable speed in the pump mode is to achieve power adjustment. The power priority control strategy can achieve rapid power adjustment, waveform is stable, and the speed response time is the same as the speed priority control strategy, so the power priority control strategy should be used in the pump mode.

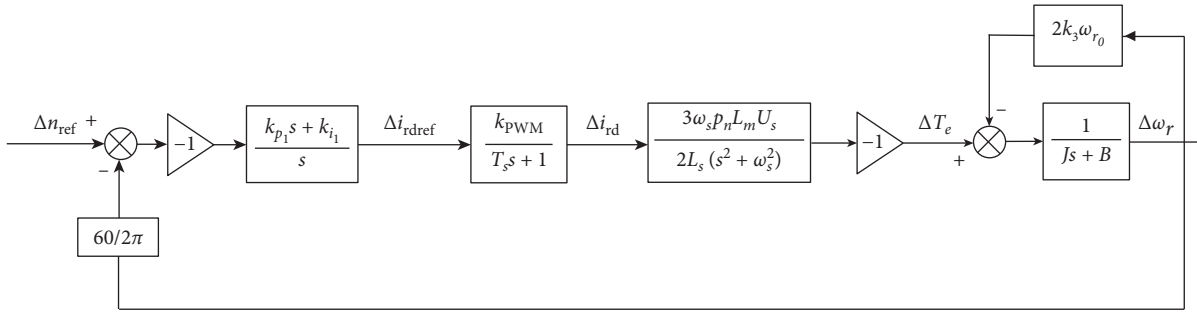

Figure 30: Linearized block diagram of the speed control closed-loop.

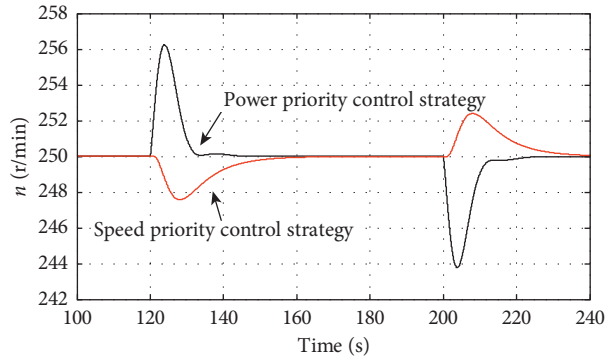

Figure 31: Speed comparison diagram when n_{ref} is unchanged and P_{ref} is changed.

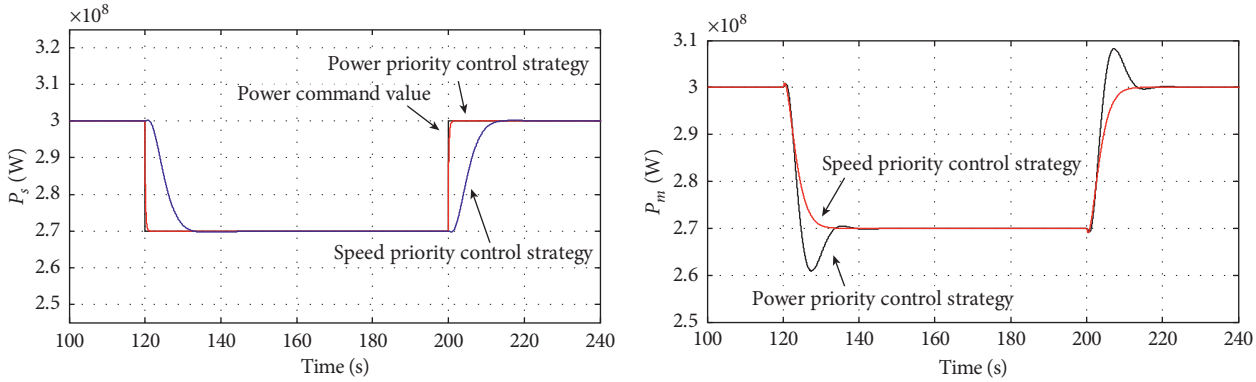

Figure 32: Active power comparison diagram when n_{ref} is unchanged and P_{ref} is changed. (a) Comparison diagram of the stator-side active power. (b) Comparison diagram of mechanical power.

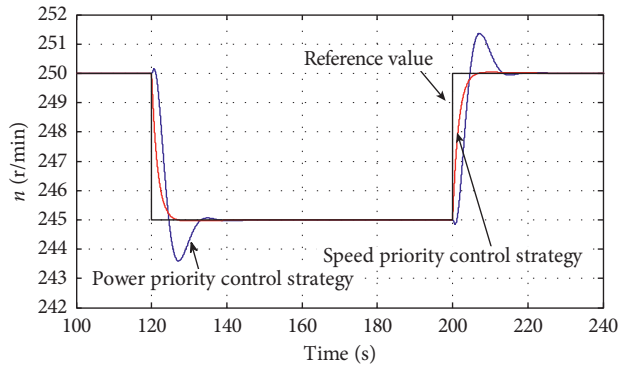

Figure 33: Speed comparison diagram when P_{ref} is unchanged and n_{ref} is changed.

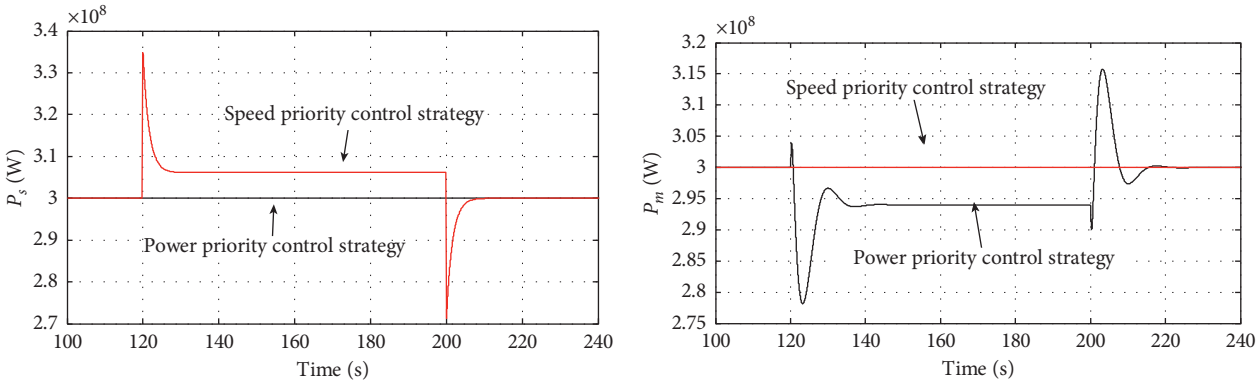

Figure 34: Active power comparison diagram when P_{ref} is unchanged and n_{ref} is changed. (a) Comparison diagram of mechanical power. (b) Comparison diagram of stator-side active power.

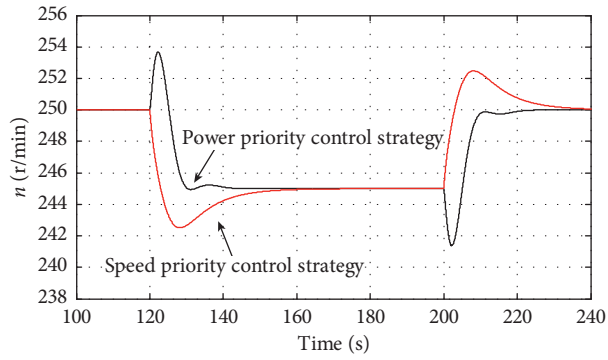

Figure 35: Speed comparison diagram when P_{ref} and n_{ref} are changed at the same time.

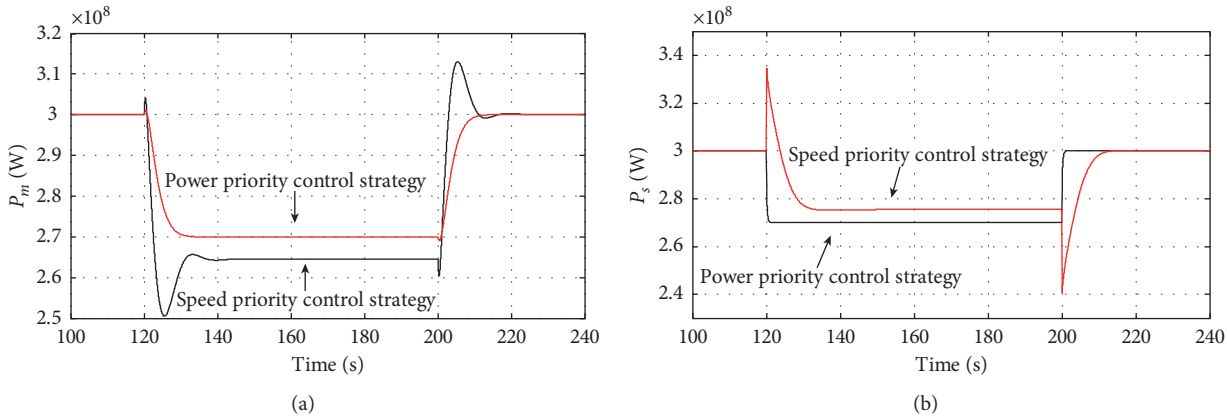

FIGURE 36: Active power comparison diagram when P_{ref} and n_{ref} are changed at the same time. (a) Comparison diagram of mechanical power. (b) Comparison diagram of stator-side active power.

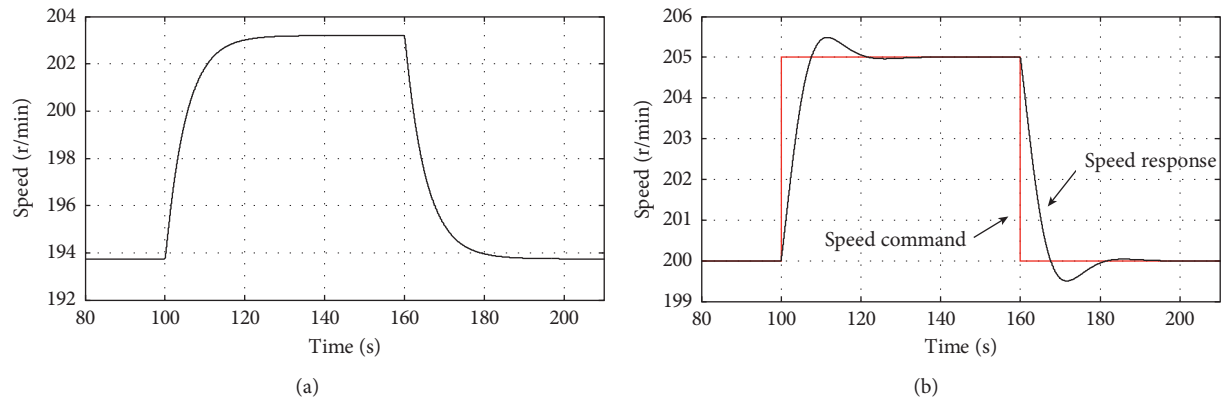

FIGURE 37: Comparison diagram of the speed. (a) Power priority control strategy. (b) Speed priority control strategy.

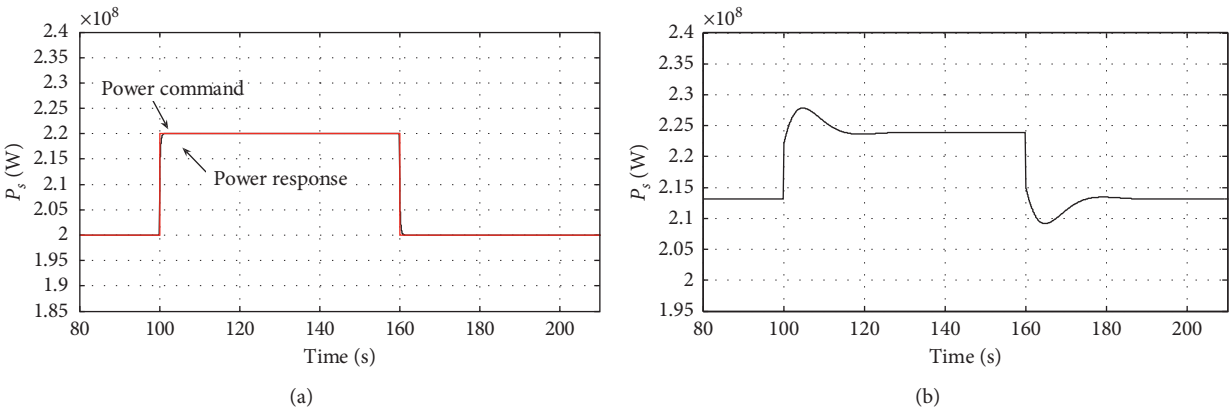

FIGURE 38: Comparison diagram of the stator-side active power. (a) Power priority control strategy. (b) Speed priority control strategy.

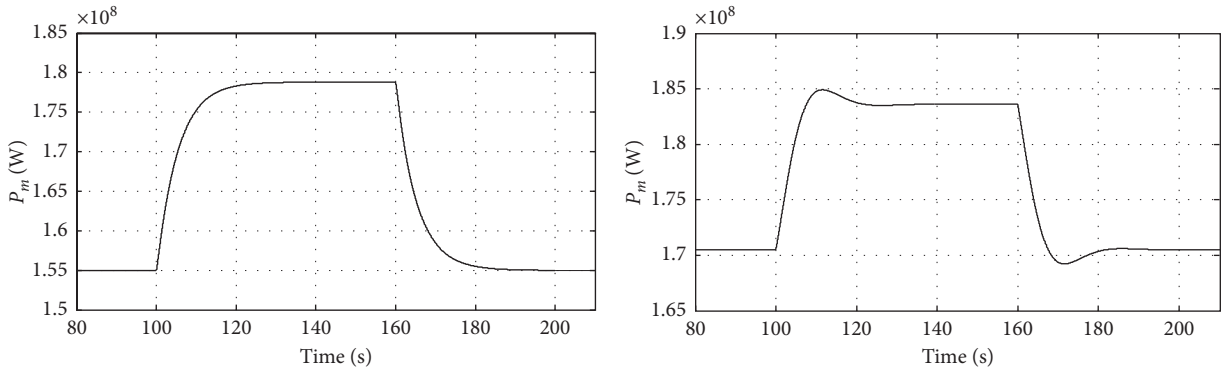

Figure 39: Comparison diagram of the pump turbine mechanical power. (a) Power priority control strategy. (b) Speed priority control strategy.

6. Conclusions

This paper first introduces the structure of a DFVSPS unit, and then the unit is modelled as blocks, including pump turbine and its guide vane opening adjustment systems, DFIM, and excitation control systems. The following two control strategies of the unit are introduced. The control system of the unit is analyzed when two control strategies are used to operate the unit in the vicinity of the rated condition in the generating mode and the pump mode. The influence of the value of the unit's own parameters on the characteristics of the control system is analyzed, and the control parameters of the system are designed to optimize the control effect. Finally, the characteristics of two control strategies in the generating mode and the pump mode are compared, and the applicable conditions for each control strategy are obtained. The relevant conclusions reached are as follows.

In the power priority control strategy, the power control closed-loop where the excitation control system is located is an independent control closed-loop, which can achieve millisecond-level power adjustment, the waveform is stable, and the control characteristics are not affected by the speed control closed-loop where the pump-turbine guide vane opening adjustment system is located. As the adjustment time is very short, it can be considered that the adjustment system of the pump turbine is triggered due to the change of speed after the power is stabilized. Therefore, it can be considered that the two control systems are decoupled and have strong stability.

The speed priority control strategy can decrease the speed response time, but due to the unit's moment of inertia, the decrease of the speed response time is not very obvious. And, the control variable is the speed. The excitation control system and the pump turbine guide vane opening adjustment system will be adjusted at the same time. The coupling between the two control systems is very strong. The stability and operating efficiency will be reduced.

When the main role of the DFVSPS unit is power regulation, whether it is running in the generating mode or the pump mode, due to the excellent response of the power priority control strategy to power command, this control strategy should be given priority consideration.

Data Availability

The data used to support the findings of this study are included within the article.

Conflicts of Interest

The authors declare that there are no conflicts of interest regarding the publication of this paper.

Acknowledgments

This study was supported by the State Key Laboratory of Alternate Electrical Power System With Renewable Energy Sources (Grant no. LAPS20010).

References

[1] P. Singh and B. Khan, "Smart microgrid energy management using a novel artificial shark optimizations," *Complexity*, vol. 2017, no. 1, 22 pages, Article ID 2158926, 2017.

[2] X. L. Su, Z. K. Zhao, Y. Si, and Y. Q. Guo, "Adaptive robust SMC-based AGC auxiliary service control for ESS-integrated PV/wind station," *Complexity*, vol. 2020, no. 2, Article ID 8879045, 2020.

[3] M. Bragard, N. Soltau, S. Thomas, and R. W. De Doncker, "The balance of renewable sources and user demands in grids: power electronics for modular battery energy storage systems," *IEEE Transactions on Power Electronics*, vol. 25, no. 12, pp. 3049–3056, 2010.

[4] M. A. Hozouri, A. Abbaspour, M. Fotuhi-Firuzabad, and M. Moeini-Aghtaie, "On the use of pumped storage for wind energy maximization in transmission-constrained power systems," *IEEE Transactions on Power Systems*, vol. 30, no. 2, pp. 1017–1025, 2015.

[5] J. Li, C. Yi, and S. Gao, "Prospect of new pumped-storage power station," *Global Energy Interconnection*, vol. 2, no. 3, pp. 235–243, 2019.

[6] M. Alizadeh Bidgoli, W. Yang, A. Ahmadian et al., "DFIM versus synchronous machine for variable speed pumped

storage hydropower plants: a comparative evaluation of technical performance," *Renewable Energy*, vol. 159, no. 5, pp. 72–86, 2020.

[7] M. Alizadeh Bidgoli, S. Atrian, W. Yang, and F. M. Gonzalez-Longatt, "Transient stability assessment of power system incorporating DFIM-based pumped storage hydropower and wind farm," *Power Systems*, pp. 131–152, 2021.

[8] M. Alizadeh Bidgoli, D. Ganjali, W. Yang, and S. Atrian, "Small signal stability improvement of pumped storage hydropower using wide area signal considering wind farm," *Wide Area Power Systems Stability, Protection, and Security*, Springer, Berlin, Germany, 2021.

[9] W. Yang and J. Yang, "Advantage of variable-speed pumped storage plants for mitigating wind power variations: integrated modelling and performance assessment," *Applied Energy*, vol. 237, no. 5, pp. 720–732, 2019.

[10] H. Aburub, S. Basnet, W. T. Jewell et al., "On the use of adjustable-speed pumped hydro storage operation in the U.S electricity market," *Journal of Energy Storage*, vol. 23, no. 6, pp. 495–503, 2019.

[11] S. Nag and K. Y. Lee, "DFIM-based variable speed operation of pump-turbines for efficiency improvement," *IFAC-PapersOnLine*, vol. 51, no. 28, pp. 708–713, 2018.

[12] J. R. Lima, G. Damm, A. Benchaib, E. Nobile, and A. Schwery, "Nonlinear control of a fully-fed variable speed pumped storage plant," *IFAC-PapersOnLine*, vol. 50, no. 1, pp. 3250–3255, 2017.

[13] W. Yang and J. Yang, "Evaluating fast power response of variable speed pumped storage plants to balance wind power variations," *Energy Procedia*, vol. 158, no. 1, pp. 6341–6346, 2019.

[14] F. Chen, C. S. Li, C. Li, D. Tan, and Z. J. Mai, "Advantage analysis of variable-speed pumped storage units in renewable energy power grid: mechanism of avoiding S-shaped region," *International Journal of Electrical Power & Energy Systems*, vol. 120, no. 9, Article ID 105976, 2020.

[15] A. Joseph and T. R. Chelliah, "A review of power electronic converters for variable speed pumped storage plants: configurations, operational challenges, and future scopes," *IEEE Journal of Emerging and Selected Topics in Power Electronics*, vol. 6, no. 1, pp. 103–119, 2018.

[16] K. Desingu, R. Selvaraj, T. R. Chelliah, and D. Khare, "Effective utilization of parallel connected megawatt three-level back-to-back power converters in variable speed pumped storage units," in *Proceedings of IEEE Industry Applications Society Annual Meeting*, Portland, OR, USA, September 2018.

[17] K. Desingu, R. Selvaraj, and T. R. Chelliah, "Control of reactive power for stabilized junction temperature in power electronic devices serving to a 250-MW asynchronous hydrogenerating unit," *IEEE Transactions on Industry Applications*, vol. 55, no. 6, pp. 7854–7867, 2019.

[18] A. Joseph, K. Desingu, R. R. Semwal, T. R. Chelliah, and D. Khare, "Dynamic performance of pumping mode of 250 MW variable speed hydro-generating unit subjected to power and control circuit faults," *IEEE Transactions on Energy Conversion*, vol. 33, no. 1, pp. 430–441, 2017.

[19] M. A. Bidgoli, H. A. Mohammadpour, and S. M. T. Bathaee, "Advanced vector control design for DFIM-based hydropower storage for fault ride-through enhancement," *IEEE Transactions on Energy Conversion*, vol. 30, no. 4, pp. 1449–1459, 2015.

[20] J. Schmidt, W. Kemmetmüller, and A. Kugi, "Modeling and static optimization of a variable speed pumped storage power plant," *Renewable Energy*, vol. 111, no. 10, pp. 38–51, 2017.

[21] A. Joseph, K. Desingu, R. R. Semwal, T. R. Chelliah, and D. Khare, "Dynamic performance of pumping mode of 250 MW variable speed hydro-generating unit subjected to power and control circuit faults," *IEEE Transactions on Energy Conversion*, vol. 33, no. 1, pp. 430–441, 2017.

[22] K. R. Vasudevan, V. K. Ramachandaramurthy, G. Venugopal, J. B. Ekanayake, and S. K. Tiong, "Variable speed pumped hydro storage: a review of converters, controls and energy management strategies," *Renewable and Sustainable Energy Reviews*, vol. 135, no. 1, 2021.

[23] T. Kuwabara, A. Shibuya, H. Furuta, E. Kita, and K. Mitsuhashi, "Design and dynamic response characteristics of 400 MW adjustable speed pumped storage unit for Ohkawachi power station," *IEEE Transactions on Energy Conversion*, vol. 11, no. 2, pp. 376–384, 1996.

[24] Y. Pannatier, C. Nicolet, B. Kawkabani, J.-J. Simond, and Ph. Allenbach, "Dynamic behavior of a 2 variable speed pump-turbine power plant," in *Proceedings of International Conference on Electrical Machines*, Tokyo, Japan, November 2009.

[25] L. Jia, H. Zhao, Z. Gao et al., "A low voltage crossing strategy for doubly-fed fan based on explicit model prediction control and improved virtual impedance," *Power Grid Technology*, vol. 45, no. 5, pp. 1716–1723, 2021.

[26] Z. Mei, *Pumped Storage Power Generation Technology*, Machinery Industry Press, Beijing, China, 2000.

[27] Z. Zuo, H. Fan, S. Liu, and Y. Wu, "S-shaped characteristics on the performance curves of pump-turbines in turbine mode-a review," *Renewable and Sustainable Energy Reviews*, vol. 60, no. 7, pp. 836–851, 2016.

[28] IEEE Working Group, "Hydraulic turbine and turbine control models for system dynamic studies," *IEEE Transactions on Power Systems*, vol. 7, no. 1, pp. 167–179, 1992.

[29] J. Liang and R. G. Harley, "Pumped storage hydro-plant models for system transient and long-term dynamic studies," in *Proceedings of IEEE PES General Meeting*, Minneapolis, MN, USA, July 2010.

[30] L. Hui, Z. Huang, H. Liu et al., "Fast power response control strategy for AC excitation pumped storage unit," *Electrical Automation Equipment*, vol. 37, no. 11, pp. 156–161+175, 2017.

[31] C. Ding, *Modeling and Nonlinear Dynamic Analysis of the Regulating System of the Frictional Turbine*, Northwest A&F University, Xianyang, China, 2013.

[32] J.-K. Lung, Y. Lu, W.-L. Hung, and W.-S. Kao, "Modeling and dynamic simulations of doubly fed adjustable-speed pumped storage units," *IEEE Transactions on Energy Conversion*, vol. 22, no. 2, pp. 250–258, 2007.

[33] P. Beires, M. H. Vasconcelos, C. L. Moreira, and J. A. Peças Lopes, "Stability of autonomous power systems with reversible hydro power plants," *Electric Power Systems Research*, vol. 158, no. 5, pp. 1–14, 2018.